

Deterministic construction of typical networks in network models

Narayan G. Sabhahit^{*,1,*} Moritz Laber^{*,1,2,†} Harrison Hartle³ Jasper van der Kolk⁴

Samuel V. Scarpino^{1,3,5,6,7,8} Brennan Klein^{1,5,9} and Dmitri Krioukov^{1,9,10,11,‡}

¹*Network Science Institute, Northeastern University, Boston, Massachusetts, USA 02115*

²*Complexity Science Hub Vienna, Metternichgasse 8, Vienna, 1030 Austria*

³*Santa Fe Institute, Santa Fe, New Mexico, USA 87505*

⁴*Department of Condensed Matter Physics, University of Barcelona, Martí i Franqués 1, E-08028 Barcelona, Spain*

⁵*Institute for Experiential AI, Northeastern University, Boston, Massachusetts, USA, 02115*

⁶*Department of Public Health and Health Sciences, Northeastern University, Boston, USA, 02115*

⁷*Khoury College of Computer Sciences, Northeastern University, Boston, USA, 02115*

⁸*Vermont Complex Systems Institute, University of Vermont, Burlington, VT, USA, 05405*

⁹*Department of Physics, Northeastern University, Boston, Massachusetts, USA 02115*

¹⁰*Department of Mathematics, Northeastern University, Boston, Massachusetts, USA 02115*

¹¹*Department of Electrical & Computer Engineering,
Northeastern University, Boston, Massachusetts, USA 02115*

It is often desirable to assess how well a given dataset is described by a given model. In network science, for instance, one often wants to say that a given real-world network appears to come from a particular network model. In statistical physics, the corresponding problem is about how typical a given state, representing real-world data, is in a particular statistical ensemble. One way to address this problem is to measure the distance between the data and the most typical state in the ensemble. Here, we identify the conditions that allow us to define this most typical state. These conditions hold in a wide class of grand canonical ensembles and their random mixtures. Our main contribution is a deterministic construction of a state that converges to this most typical state in the thermodynamic limit. This construction involves rounds of derandomization procedures, some of which deal with derandomizing point processes, an uncharted territory. We illustrate the construction on one particular network model, deterministic hyperbolic graphs, and its application to real-world networks, many of which we find are close to the most typical network in the model. While our main focus is on network models, our results are very general and apply to any grand canonical ensembles and their random mixtures satisfying certain niceness requirements.

I. INTRODUCTION

Modeling real-world networks is one of the core research activities in network science [1], where it is often tempting to say that a particular real-world network appears “to come from” a particular model [2–4]. Such statements usually mean that the real-world network in question appears to be (close to) a *typical* network in the model under consideration. This is usually supported by generating many random networks in the model, and by comparing their averaged properties of interest to the corresponding properties of the real network.

However, it is often desirable to “suppress noise,” and to work not with a zoo of random networks, but with just one—the “most representative” or “most typical” one—constructed deterministically. In network science, representative graph constructions are needed to boost reliability of statistical inference, to suppress or control sample-to-sample fluctuations, and for many other purposes [1, 5–8]. More generally, the importance of representative typical states, as opposed to averages over

many random realizations, has been emphasized repeatedly in many areas of statistical physics ranging from quantum typicality and thermalization to the breakdown of self-averaging near critical points and in disordered media [9–14]. In more data-driven domains such as machine learning, stochasticity is a key source of irreproducibility, so the push towards more deterministic, reproducible benchmarks has become a major priority [15–17].

The deterministic construction of typical networks in random network models—a task reminiscent of the construction of expanders [18] and pseudorandom graphs [19–21]—requires a definition of typical networks. The definition of network typicality [22, 23] is problematic if the probability $\mathbb{P}(G)$ of networks G in the model is unknown or intractable, as is typically the case with network models defined by some (complicated) network-construction rules. Typical values of network properties in such models can be computed, but typical networks *per se* cannot be defined because a network with typical values of some properties may have atypical values of some other unchecked properties [25]. Nor does it make much sense to ask for the “most typical” network in models with high degeneracy of typical sets. In the canonical Erdős-Rényi $\mathcal{G}(n, p)$ model [26], for instance, the standard definition of typical sets based on the asymptotic equipartition property [27, 28] says that the most typical networks are the ones with n nodes and $m = \lfloor Np \rfloor$ links, where $N = \binom{n}{2}$ and $\lfloor \cdot \rfloor$ is the nearest integer function.

* sabhahit.n@northeastern.edu

† laber.m@northeastern.edu

‡ dima@northeastern.edu

* These authors contributed equally

However, any of these many $\binom{N}{m}$ networks is equally typical, leaving substantial ambiguity in the selection of a single deterministic representative.

Here, we develop a general definition of *typical networks* in a model, and discuss a class of network models—equivalent to grand canonical ensembles in statistical physics—where this definition makes sense and allows for the selection of a unique *most typical network*. We also develop methods to construct such networks deterministically in a computationally efficient fashion, and show how these methods work in application to a particular grand canonical network model and to real-world network data.

II. NETWORK TYPICALITY

The simplest case where a definition of the most typical network is possible is when the following conditions are satisfied:

1. the probability $\mathbb{P}(G)$ of networks G in a model depends on G only via some network properties \mathbf{f} : $\mathbb{P}(G) = \mathbb{P}[\mathbf{f}(G)]$;
2. the distribution $\mathbb{P}(v)$ of the values v of these properties in the model, $\mathbb{P}(v) = \sum_{G \in \mathcal{G}} \mathbb{P}(G) \delta(\mathbf{f}(G), v)$, is sharply peaked (self-averaging); and
3. the very top of this peak is populated by just one network G^* .

Such G^* is then the most typical network in the model, Fig. 1. Condition (2) ensures there is a typical set, condition (3) says there is the most typical element in this set, while condition (1) allows us to extend the notion of typicality from network properties to networks *per se* because it ensures that nothing other than these properties matters in the model.

Condition (3) is satisfied if properties $\mathbf{f}(G)$ —called *sufficient statistics* in statistics—are real-valued, reducing degeneracy. Conditions (1,2) are satisfied in a multitude of models. Here, we focus on *grand canonical* models. This is one of the best-studied—both in statistical physics and network science [22, 29]—class of models in which the conditions above are satisfied, and which is particularly attractive for statistical analysis thanks to its maximum-entropy properties. This is the key feature of *exponential random graph models* (ERGMs), of which grand canonical models are a special case (Appendix A).

In grand canonical models, links between nodes i and j form independently with the Fermi-Dirac probabilities

$$p_{ij} = \frac{1}{e^{\beta(\varepsilon_{ij}-\mu)} + 1} = \frac{1}{e^{\alpha+\beta\varepsilon_{ij}} + 1}, \quad (1)$$

where the inverse temperature β and chemical potential μ are the model parameters, $\alpha = -\mu\beta$, and ε_{ij} are energies of particle states $\{i, j\}$ —particles are links. The models

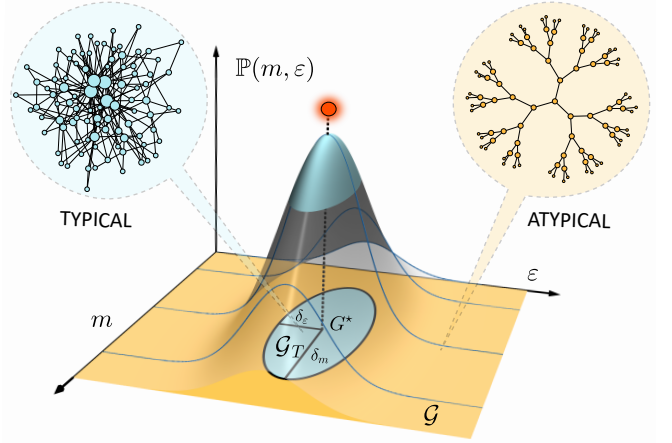


FIG. 1. **Network typicality definition.** In any grand canonical model of networks, Eq. (2), the distribution $\mathbb{P}(m, \varepsilon)$ of the number of links $m(G)$ and energy $\varepsilon(G)$ of network G is sharply peaked. A typical set \mathcal{G}_T is the set of networks whose values of m and ε are within the $(\delta_m, \delta_\varepsilon)$ -neighborhood around their expected values $(\bar{m}, \bar{\varepsilon})$, Eq. (3), while the most typical network $G^* = \operatorname{argmin}_{G \in \mathcal{G}} (|m(G) - \bar{m}| + |\varepsilon(G) - \bar{\varepsilon}|)$ is the network which is closest to the top of the peak. This network is unique with high probability if energy $\varepsilon(G)$ is a real-valued function.

in this class differ in definitions of link energy. The probability $\mathbb{P}(G)$ of network G in any grand canonical model is [22]

$$\mathbb{P}(G) = e^{-\alpha m(G) - \beta \varepsilon(G)} / \mathcal{Z}, \quad (2)$$

so the sufficient statistics $\mathbf{f}(G)$ are the number of particles (links) $m(G)$ in network G , and G 's energy, the sum of its link energies $\varepsilon(G) = \sum_{i,j} \varepsilon_{ij} G_{ij}$, where $\{G_{ij}\}$ is G 's adjacency matrix. The partition function \mathcal{Z} is the normalization coefficient. As in any grand canonical ensemble [29], the $\mathbb{P}(G)$ in Eq. (2) maximizes Shannon entropy across all other models with the same expected values of the number of links \bar{m} and network energy $\bar{\varepsilon}$ (Appendix A).

The distributions of both the number of particles and energy are known to be self-averaging in grand canonical ensembles [30]. Therefore, we define a $(\delta_m, \delta_\varepsilon)$ -typical set of networks as

$$\mathcal{G}_T = \left\{ G \in \mathcal{G}_n : \frac{|m(G) - \bar{m}|}{m_n} < \delta_m, \frac{|\varepsilon(G) - \bar{\varepsilon}|}{m_n} < \delta_\varepsilon \right\}, \quad (3)$$

where \mathcal{G}_n is the set of all networks of size n , and m_n is the asymptotic scaling of \bar{m} with n ($\bar{m} \sim m_n$). The self-averaging properties of grand canonical ensembles ensure that in the thermodynamic limit $n \rightarrow \infty$, the bulk of the probability mass is concentrated on the typical set: for any $\delta_\varepsilon, \delta_m > 0$, $\mathbb{P}(G \in \mathcal{G}_T) \rightarrow 1$. And if energies ε_{ij} are all different real numbers, then all different networks G have different energies $\varepsilon(G)$, so the top of the peak is occupied by one network—the most typical one in Fig. 1. The question is how to find it.

III. CONSTRUCTING TYPICAL NETWORKS

A. Grand canonical models

Selecting the most typical value m^* of the number of links in a grand canonical model is easy: m^* is the closest integer to the expected number of links $\bar{m} = \sum_{i<j} p_{ij}$, $m^* = \lfloor \bar{m} \rfloor$. Yet if the network size n is large, then the brute-force search for the network G^* minimizing the network energy difference $|\varepsilon(G) - \bar{\varepsilon}|$ across the resulting $\binom{N}{m^*}$ possible networks is computationally prohibitive, akin to the NP-complete subset sum problem [31] and knapsack problem [32].

To address this problem, we devise a deterministic link creation process that emulates random sampling of links (i, j) with probabilities p_{ij} . It is presented in Fig. 2(a). The process simply overlays the matrix \mathbf{p} of connection probabilities $\{p_{ij}\}$ over a regular lattice with m^* vertices, thus building a unique network $G_{\mathbf{p}}$ for any \mathbf{p} , not necessarily grand canonical (1). However, if \mathbf{p} is grand canonical, then we show in Section IV that the energy of constructed networks $\varepsilon(G_{\mathbf{p}})$ converges to its expected value $\bar{\varepsilon}$, implying that the networks themselves converge to the most typical network, $G_{\mathbf{p}} \rightarrow G^*$.

To show this convergence, we need to be able to increase the network size n in a systematic fashion. The easiest way to do so is in the context of hidden variable network models [35–37], an extremely general and well-studied class of models encompassing as special cases many quintessential network models in network science (Appendix B). One complication is that in these models, link energies are not fixed, but random

$$\varepsilon_{ij} = \phi(x_i, x_j), \quad (4)$$

where ϕ is some fixed function of random hidden variables x_i of nodes i . The resulting models are thus not grand canonical, but probabilistic mixtures of those, which we call *hypercanonical models* since random model parameters are called hyperparameters in statistics [38]. But then, for our typical network construction to be deterministic, we have to derandomize hidden variables x_i first. We address this task next.

B. Hypercanonical models

Without much loss of generality, we can assume that hidden variables x_i are independent uniformly distributed random variables in the unit d -cube, $x_i \sim U([0, 1]^d)$. (If they are not, we can map them to $U([0, 1]^d)$ via their inverse cumulative distribution function (CDF), adjusting the function ϕ accordingly.) The question is how to derandomize n random points in the unit cube, known as the binomial point process (PPP) as $n \rightarrow \infty$ [39].

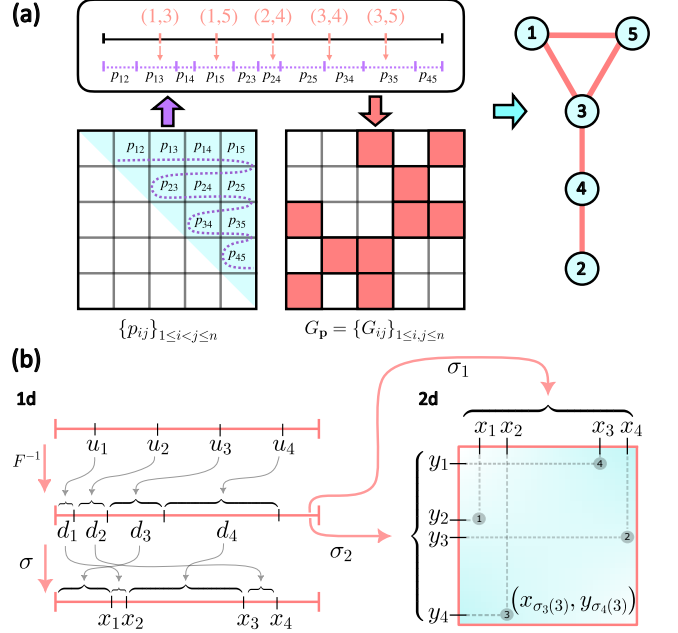


FIG. 2. **Deterministic construction of typical networks.** (a) **Grand canonical derandomization.** The connection probability matrix $\mathbf{p} = \{p_{ij}\}_{i<j}$ is first flattened into an interval of length $\bar{m} = \sum_{i<j} p_{ij}$ composed of subintervals of lengths p_{ij} as shown in the figure. The whole interval is then overlaid with an equally spaced one-dimensional lattice of the same length and with $m^* = \lfloor \bar{m} \rfloor$ internal vertices. These vertices hit m^* subintervals p_{ij} . The derandomized network $G_{\mathbf{p}}$ consists of those links (i, j) whose subintervals are hit. (b) **Hypercanonical derandomization.** To derandomize the random sprinkling of n points on the unit interval, the distances between consecutive points are first set to $d_i = -(1/n) \ln(1 - u_i)$ using the inverse CDF method [33] applied to the inverse CDF of the exponential distribution of rate n evaluated at the regular lattice $u_i = (i - 1/2)/n$, $i \in [n]$. These distances are then shuffled using a pseudorandom permutation function σ acting on indices i , so the coordinate of point i is set to $x_i = x_{i-1} + d_{\sigma(i)}$, where $x_0 = 0$. In higher dimensions d , the same permutation function is used several times with different seeds— σ_1, σ_2 in $d = 2$ —to shuffle the distances d_i between consecutive coordinates in different dimensions: $x_i = x_{i-1} + d_{\sigma_1(i)}$, $y_i = y_{i-1} + d_{\sigma_2(i)}$. It is used then again— σ_3, σ_4 —to destroy the correlations between the (x, y) -coordinates of the same point: $(x_i, y_i) = (x_{\sigma_3(i)}, y_{\sigma_4(i)})$. In this paper, permutations σ_s , $s \in [2d]$, are defined via the *multiplicative congruential generator* (MCG) [34]: σ_s is the permutation that sorts the pseudorandom MCG numbers $\{b_k\}_{k=n(s-1)+1}^{ns}$ in the increasing order, where $b_{k+1} = ab_k \bmod c$, $a = 7^5$, $b_0 = 42$, and $c = 2^{31} - 1$.

This question does not have a unique answer since it depends on what properties of the PPP we want to preserve in our derandomization, reminiscent of the choice of distinguisher in pseudorandomness [19–21]. Here, we choose to preserve the distances between nearest points in a PPP, since these distances are one of the most basic definitive properties of PPPs [39]. In a 1-

dimensional PPP of rate n , the distances d_i between consecutive points i on the real line are independent exponentially distributed random variables with rate n . The inverse CDF of the exponential distribution of rate n is $F^{-1}(x) = -(1/n)\ln(1-x)$. Therefore, to derandomize the independent sampling of d_i 's from the exponential distribution, we simply set them to $d_i = F^{-1}(u_i)$, where $u_i = (i-1/2)/n$, $i \in [n]$, is a regular lattice on $[0, 1]$. The choice of the $1/2$ shift in it is justified in Appendix C. We then use a pseudorandom function—several times in higher dimensions—as shown in Fig. 2(b), to scramble all the unwanted correlations that are not present in a PPP. In Appendix D we show that this deterministic process reproduces the distances not only between nearest points but also between two random points in $1d$ and $2d$ PPPs.

As soon as hidden variables are derandomized, the link energies (4) become fixed, and so are the link existence probabilities (1). This means that for each network size n , we now have a unique network $G_{n,\phi}$, which we claim converges to the most typical network G^* in the model, $G_{n,\phi} \rightarrow G^*$. We show this next.

IV. CONVERGENCE TO THE MOST TYPICAL NETWORK

To demonstrate the aforementioned convergence, we select one particular hypercanonical model—random hyperbolic graphs [40]. We choose this model because its energy function is real-valued, so the most typical network is well-defined. Another motivation to consider this model is that it attracted significant research attention over past decades in as diverse disciplines as machine learning, neuroscience, or Internet routing [41], thanks to its ability to capture a collection of definitive properties of many real-world networks [41]. Yet another reason to consider this model is that it encompasses several quintessential network models as its limiting regimes [42].

In the model, the hidden variables x_i are the coordinates of points sprinkled randomly over a hyperbolic disc, while energies ε_{ij} are hyperbolic distances between those points. In addition to the grand canonical parameters α, β controlling the expected number of links and energy—both scaling as $\mathcal{O}(n)$ in the model ($\bar{m} \sim \bar{\varepsilon} \sim m_n = n$)—the model has one more parameter γ , the tail exponent of the power-law node degree distribution. Further details are in Appendix E.

Since the model is not grand canonical but hypercanonical, we cannot rely on the known facts [30] that sufficient statistics, the number of particles and energy, are self-averaging in any grand canonical ensemble. We have to show that the number of links and energy are self-averaging in our hypercanonical model as well, thus satisfying the second concentration requirement in Section II. We show this in Fig. 3(a,b) and Appendix F, where we derive the following scaling of the coefficient of

variations $C_V(n)$ for these two properties in the model:

$$C_V(n) = \mathcal{O}\left(n^{-\min\{1/2, (\gamma-2)/(\gamma-1)\}}(\ln(n))^{\mathbb{1}\{\gamma=3\}/2}\right), \quad (5)$$

where $\mathbb{1}(\cdot)$ is the indicator function. This implies that $C_V(n) \rightarrow 0$ for any $\gamma > 2$, so the distributions of m and ε are sharply peaked. Since they are sharply peaked, the definitions of (most) typical networks in grand canonical models in Section II extend to this hypercanonical model as well.

Finally, Fig. 3(c,d) shows the aforementioned convergence $G_{n,\phi} \rightarrow G^*$ of the deterministic hyperbolic graphs (DHGs) $G_{n,\phi}$ to the most typical graph G^* in the random hyperbolic graph (RHG) model. The DHGs are constructed as discussed in Section III. The code is available at [43]. Appendix G documents other model-specific details, one of which is that the number of links in DHGs matches its expected value exactly for any n as Fig. 3(c) demonstrates. Figure 3(d) shows the convergence of the other sufficient statistics, energy, to its expected value as n increases. These two convergences, coupled with the self-averaging of the both sufficient statistics, ensure that the graphs themselves converge to the most typical graph. As a consequence, all properties of DHGs converge to their expected values as well. The two most basic properties—the degree distribution and clustering—are shown in Fig. 3(e,f).

V. TYPICALITY OF REAL-WORLD NETWORKS

One natural application of the developed framework, mentioned in the introduction, is the assessment of how typical a given real-world network is in a given model. For such assessments, one needs to compare two networks—a real-world one and the most typical one in the model. There are many ways to compare two networks, none of which is ultimately the best. One option is to evaluate one or many graph similarity metrics on the two networks. For a recent review of such metrics, we refer to [45, 46]. Here, instead of evaluating any of such distances, we showcase graph comparisons more directly via measuring a collection of basic properties of two networks, shown in Fig. 4. We observe that according to these fundamental properties, the Internet and the Cora citation networks are fairly close to the most typical DHG network.

In Appendix H, we present the results of such measurements applied to a total of seventeen networks from different domains. We find that in many social, technological, and biological networks, the degree distribution, clustering, distance distribution, betweenness centrality, and other properties are close to the ones of the most typical DHG network. In contrast, the distance distribution of transportation networks, such as street and urban public transport networks, that are confined to Euclidean space and therefore are large worlds, are far

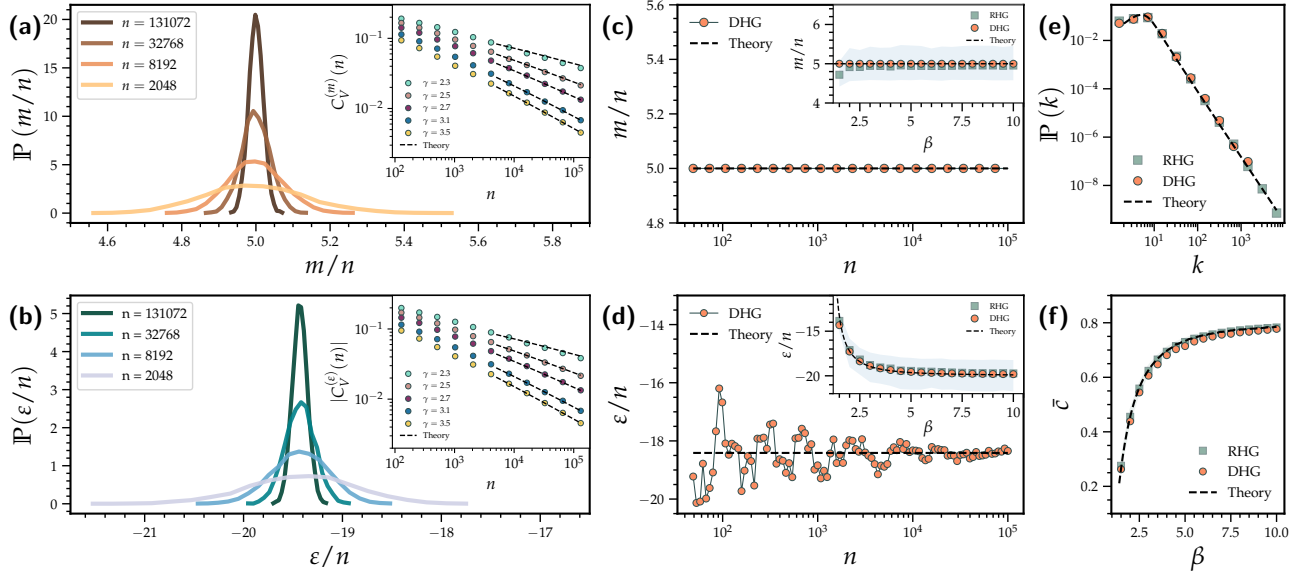


FIG. 3. **Self-averaging and convergence.** (a,b) The empirical distributions of the rescaled number of links $m(G)$ and energy $\varepsilon(G)$ of the random hyperbolic graphs (RHGs) G (Appendix E) are shown for increasing graph sizes n , and parameter values $\bar{\kappa} = 10$, $\beta = 4$, and $\gamma = 3.7$. The insets show the empirical coefficients of variation $C_V(n)$ (colored circles) and the distributions of m and ε for different values of n and γ , versus the analytical predictions (black dashed lines) in Eq. (5). (c,d) The values of the rescaled number of links $m(G)$ and energy $\varepsilon(G)$ of the deterministic hyperbolic graphs (DHGs) G (Appendix G) are shown for increasing graph sizes n , and parameter values $\bar{\kappa} = 10$, $\beta = 2.5$, and $\gamma = 2.7$. The black dashed lines are the theoretical expected values. The insets show these properties as functions of the inverse temperature β for both DHGs and RHGs with the same parameter values and $n = 10^4$. The green squares are the RHG average values, and the shades are the 95 percentiles computed over 10^3 RHG realizations. (e,f) The degree distribution and the average local clustering coefficient of DHGs and RHGs with the same parameter values as in (c,d).

from the ones of the most typical DHG, which is a small world. Across domains, we observe that larger networks are more closely aligned with the most typical DHG network, but even small networks can sometimes have properties surprisingly similar to the ones of the most typical DHG.

Summarizing, the most typical deterministic hyperbolic graph, with its three parameters α, β, γ , two of which (α, β) are the standard grand canonical ones, captures well a range of fundamental network properties—some of which, like betweenness or edge multiplicity distributions, are quite non-trivial—in many real-world networks coming from different domains, albeit with notable exceptions mentioned above.

VI. DISCUSSION

The last observation in the previous section highlights the following open question: what other properties do we get “for free” in the most typical state in a model as defined in Section II? For example, the most typical deterministic hyperbolic graph has the most typical values of the number of links (α), energy (β), and degree distribution tail (γ), yet what other network properties in this graph have their typical values as well? If the graph was random, this question could be answered by a variety of

methods including the large deviation theory. It is less clear how to approach this question given that the graph is deterministic.

Potential applications of the developed framework are definitely not limited to the motivating one discussed in the previous section. One class of such applications can be called *derandomized or deterministic statistical inference*. It would work as follows. Observe that for a given model, our framework establishes a function from the model parameter space to the space of graphs. Any combination of the parameter values corresponds to only one deterministic graph, the most typical one in the model with these parameter values. Therefore, the method is a powerful parameter inference and model selection tool. Indeed, for a given collection of network properties or graph similarity metrics, one can simply find the parameter values that minimize the corresponding graph similarity metric between a given (real-world) network and typical networks in the model. We, in fact, use this approach for parameter inference to recover a set of model parameters in Appendix H. The model selection step compares these similarity metrics between a given (real-world) network and most typical networks (with inferred parameters) in different models. The one that minimizes the distance describes the data best, according to this choice of graph distance. The conceptually closest approaches to this programme are the minimum description length

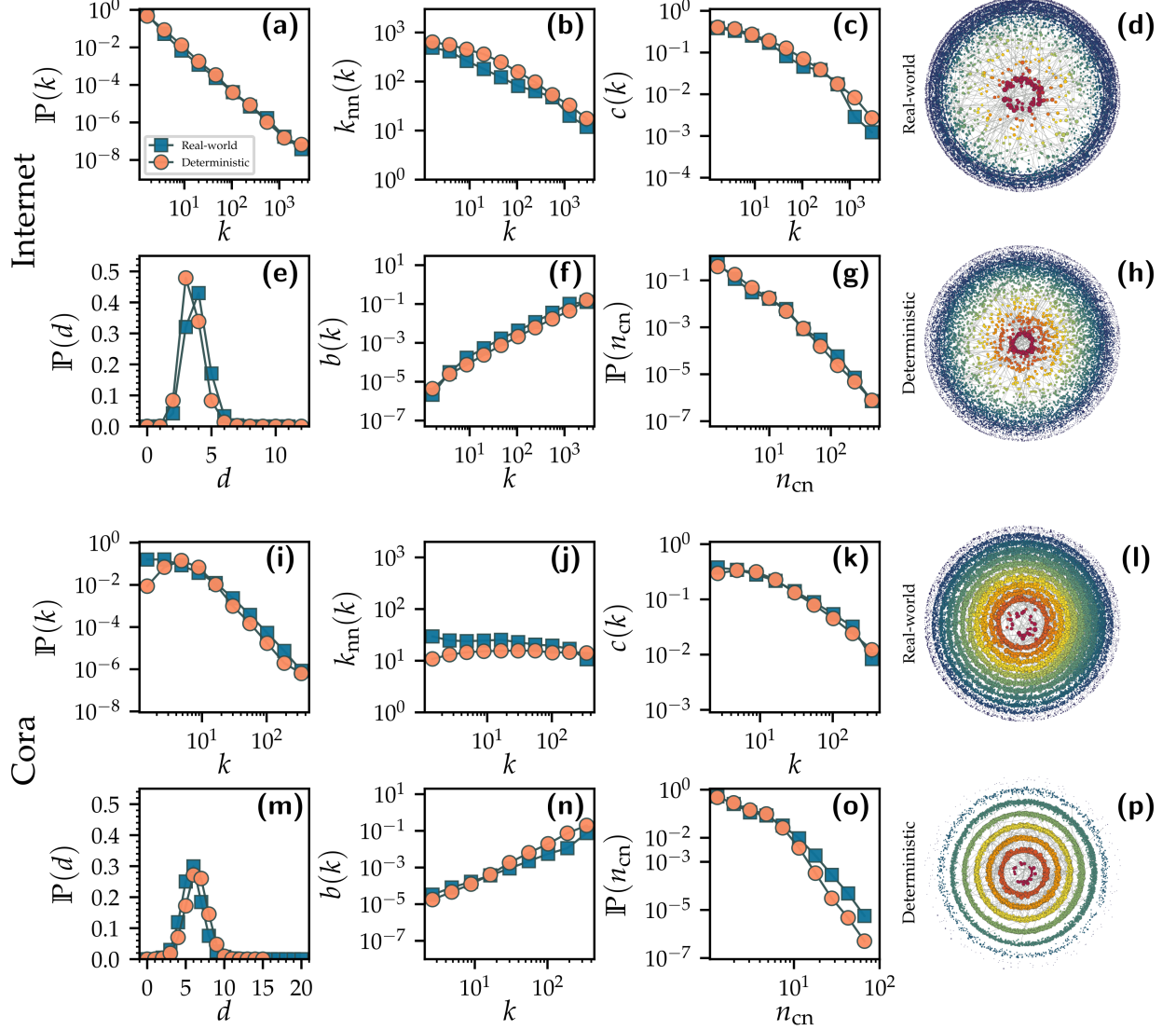


FIG. 4. **Typicity of real-world networks.** The figure displays a collection of network properties—degree distribution $\mathbb{P}(k)$ (panels (a), (i)), average nearest neighbor degree $k_{nn}(k)$ of k -degree nodes (panels (b), (j)), average local clustering $c(k)$ of k -degree nodes (panels (c), (k)), distribution $\mathbb{P}(d)$ of shortest-path distances d (panels (e), (m)), average betweenness $b(k)$ of k -degree nodes (panels (f), (n)), distribution $\mathbb{P}(n_{cn})$ of the number of common neighbors n_{cn} of pairs of connected nodes, a.k.a. edge multiplicity [44] (panels (g), (o)), of two real-world networks (blue squares) and their deterministic hyperbolic counterparts (orange circles). The real-world networks are the Internet at the autonomous system level (the upper two rows) and the Cora citation network (the lower two rows), documented as `internet_as` and `cora` in Appendix H, which also details their visualizations in panels (d), (h), (l), (p).

principle [47] and algorithmic statistics [48].

More importantly, the developed framework is very general, definitely not just limited to the realm of networks, as it applies to any grand canonical or hypercanonical ensembles satisfying the minor niceness conditions discussed in Section II. These conditions are typically satisfied in most paradigmatic systems. While grand canonical ensembles are very common in statistical physics, hypercanonical ones are less so, yet they

still appear in many mainstream systems, such as spin glasses with frozen disorder [49].

As a final note, to derandomize hypercanonical ensembles, we had to derandomize the Poisson point process in Section IIIB. Derandomization of point processes appears to be a poorly explored territory that would be interesting to investigate on more rigorous grounds. Potential applications may turn out to be as abundant and fruitful as with derandomization of other discrete ran-

dom structures in information theory and machine learning [18, 50].

ACKNOWLEDGMENTS

N.G.S. and D.K. acknowledge the support of NSF Grant No. CCF-2311160. J.v.d.K. and B.K. acknowledge the support of the AccelNet-MultiNet program, a project of the National Science Foundation (Awards #1927425 and #1927418). H.H. acknowledges support from the Santa Fe Institute. H.H., S.V.S., and B.K. acknowledge the support of a grant from the John Templeton Foundation (61780). S.V.S. acknowledges the support of NSF Grant No. FAIN-2133740. Any opinions, findings, conclusions, or recommendations expressed in this material are those of the author(s) and do not necessarily reflect the views of the funders, including the National Science Foundation and John Templeton Foundation.

Appendix A: Exponential random graph models

A random graph model is defined as a probability distribution, denoted $\mathbb{P}(G)$, over the set \mathcal{G} of all possible labeled graphs G of size n . On many occasions, we are given a graph G^* and tasked with coming up with a model that reproduces a set of graph properties of interest, denoted $\mathbf{f}(G^*)$, e.g., the number of edges, the degree sequence, or the number of triangles. In such a scenario, it is desirable to develop a model that reproduces the given constraints but is otherwise maximally random; otherwise, the model injects extraneous information. This view is known as the maximum entropy principle [29, 51], whereby among all distributions satisfying the constraints, the one selected as a model should maximize Shannon entropy,

$$S[\mathbb{P}] = - \sum_{G \in \mathcal{G}} \mathbb{P}(G) \log \mathbb{P}(G). \quad (\text{A1})$$

Such a model can then be used as a *null model* for G^* , the properties of which, beyond those constrained, can be compared against those of G^* . If major differences are observed, it indicates the presence of statistical mechanisms beyond those implied by the constraints; if not, the constraints chosen are considered sufficiently explanatory.

If the constraints are sharply enforced, then we have a *microcanonical ensemble* and the form of $\mathbb{P}(G)$ is just a uniform measure over the set of all graphs that satisfy the constraint exactly, i.e., drawn uniformly from the set $\{G \in \mathcal{G} : \mathbf{f}(G) = \mathbf{f}(G^*)\}$. If the constraints are enforced to be satisfied only in expectation,

$$\bar{\mathbf{f}} = \sum_{G \in \mathcal{G}} \mathbf{f}(G) \mathbb{P}(G) = \mathbf{f}(G^*), \quad (\text{A2})$$

then we have a *canonical ensemble*; note the requirement of $\sum_{G \in \mathcal{G}} \mathbb{P}(G) = 1$ is an additional constraint on the values of $\{\mathbb{P}(G)\}_{G \in \mathcal{G}}$. This constrained optimization problem is solved using the method of Lagrange multipliers, resulting in Gibbs/Boltzmann exponential family distribution [22],

$$\mathbb{P}(G) = \frac{e^{-\boldsymbol{\lambda} \cdot \mathbf{f}(G)}}{\sum_{\tilde{G} \in \mathcal{G}} e^{-\boldsymbol{\lambda} \cdot \mathbf{f}(\tilde{G})}}, \quad (\text{A3})$$

where $\boldsymbol{\lambda}$ is a vector of Lagrange multipliers whose values must be set to $\boldsymbol{\lambda} = \boldsymbol{\lambda}^*$ such that the soft constraint $\bar{\mathbf{f}} = \mathbf{f}(G^*)$ is realized.

Since the value of $\mathbb{P}(G)$ depends on the graph G only through $\mathbf{f}(G)$, the properties $\mathbf{f}(G)$ are called *sufficient statistics* of the model. Formally, Eq. (A3) are the entropy maximizing distributions subjected to the constraints $\mathbf{f}(G^*)$ called *exponential random graph models* (ERGMs) [22, 29, 52, 53]. ERGMs and the maximum entropy formalism in general have been successful in modeling patterns of activity in neuronal circuits [54], testing various hypotheses regarding the tie-formation mechanism in social networks [55, 56], and as null models in network science [1, 57].

A particular class of ERGMs which is of interest to us here is the class of *grand canonical* models [22, 30, 58, 59], where two nodes are connected independently with probability

$$p_{ij} = \frac{1}{e^{\beta(\varepsilon_{ij} - \mu)} + 1} = \frac{1}{e^{\alpha + \beta\varepsilon_{ij}} + 1}, \quad (\text{A4})$$

where β (inverse temperature) and μ (chemical potential) are the model parameters, $\alpha = -\mu\beta$, and ε_{ij} are link energies. Letting $G_{ij} \in \{0, 1\}$ denote the adjacency matrix elements of G , the graph probability mass function is given by,

$$\begin{aligned} \mathbb{P}(G) &= \prod_{1 \leq i < j \leq n} p_{ij}^{G_{ij}} (1 - p_{ij})^{1 - G_{ij}}, \\ &= \exp \left(\sum_{1 \leq i < j \leq n} G_{ij} \log \left(\frac{p_{ij}}{1 - p_{ij}} \right) + \log(1 - p_{ij}) \right), \\ &= \frac{\exp(-\alpha m(G) - \beta \varepsilon(G))}{\mathcal{Z}}, \end{aligned} \quad (\text{A5})$$

where $m(G) = \sum_{i < j} G_{ij}$ is the number of edges in graph G , $\varepsilon(G) = \sum_{i < j} G_{ij} \varepsilon_{ij}$ is its energy, and $\mathcal{Z} = \prod_{1 \leq i < j \leq n} 1/(1 - p_{ij})$ is the partition function. Comparing the above equation with Eq. (A3), it is clear that the grand canonical model is an entropy-maximizing distribution subjected to the constraint on the expected values of the number of edges and energy. In other words, the grand canonical model is an ERGM in which the sufficient statistics are the number of edges and energy.

Appendix B: Hidden variable network models

Hidden variable network models (HVNMs) are a widely studied class of random network models characterizing how heterogeneously distributed node-variables (hidden variables (HVs)) can give rise to various patterns of network connectivity [35–37]. Graphs sampled from HVNMs arise through two stages of randomness:

- a) each node $i \in [n] = \{1, 2, \dots, n\}$ gets a random hidden variable $h_i \in \mathcal{X}$ in some space \mathcal{X} sampled independently from some probability density $v(h)$;
- b) edges form pairwise-independently with probability $p_{ij} = g(h_i, h_j)$ where $g : \mathcal{X}^2 \rightarrow [0, 1]$ is the connection probability function.

Consequently, the hidden variable configuration $H = (h_i)_{i=1}^n \in \mathcal{X}^n$ has a joint probability density of the form $\rho(H) = \prod_{i=1}^n v(h_i)$. Without much loss of generality, one may set $\mathcal{X} = [0, 1]^d$ and $v = U([0, 1]^d)$ in the case of d -dimensional HVs, since we can often map this hidden variable configuration to the intended hidden variable space via the inverse transform sampling [33, 60]. In this setting, the probability of a network given H is,

$$\begin{aligned} \mathbb{P}(G|H) &= \prod_{1 \leq i < j \leq n} p_{ij}^{G_{ij}} (1 - p_{ij})^{1 - G_{ij}}, \\ &= \frac{e^{-\sum_{i < j} \lambda_{ij} G_{ij}}}{\mathcal{Z}}, \end{aligned}$$

where $\lambda_{ij} = \ln \left(\frac{1 - p_{ij}}{p_{ij}} \right)$, $\mathcal{Z} = \prod_{1 \leq i < j \leq n} \left(\frac{1}{1 - p_{ij}} \right)$. (B1)

Thus, any HVNM conditioned on the hidden-variable configuration H (i.e., an HVNM with a specified “frozen” configuration H) is an ERGM (Appendix A) with $\binom{n}{2}$ pairwise constraints of the form

$$\bar{G}_{ij} = g(h_i, h_j). \quad (\text{B2})$$

However, some choices of specific functional forms of the connection probability function $g(\cdot)$ —including the grand canonical one in Eq. (A4)—collapse the $\binom{n}{2}$ individual edge indicator sufficient statistics into only a few aggregated sufficient statistics, like the number of edges and energy in the grand canonical case.

The probability of graph G in an HVNM is

$$\mathbb{P}(G) = \int_H \mathbb{P}(G|H) \rho(H) dH. \quad (\text{B3})$$

Therefore, HVNMs are probabilistic mixtures of ERGMs, $\mathbb{P}(G|H)$, with mixing distribution $\rho(H)$. We refer to such distributions as *hypercanonical ensembles*, so all HVNMs are hypercanonical.

By appropriately choosing the hidden-variable distribution $\rho(\cdot)$ and the connection-probability function $g(\cdot)$, hidden-variable network models (HVNMs) can encompass a broad spectrum of paradigmatic network models,

including the Erdős-Rényi random graph model [26, 61], (hypersoft) configuration model [62], stochastic block model [63], latent-space models [40, 41, 64–66], and many others.

Appendix C: Justification for the lattice shift

In this section, we motivate the choice of shifting the regular lattice, $u_i = (i - z)/n$, horizontally by $z = 1/2$, in the deterministic sprinkling process (outlined in Sec. III B). The coordinate of point i in the $1d$ deterministic sprinkling process on the unit interval is given by,

$$x_i = -\frac{1}{n} \sum_{l=1}^i \ln(1 - u_{\sigma(i)}), \quad (\text{C1})$$

where $\sigma : [n] \rightarrow [n]$ is a pseudo-random permutation function. We want these deterministically sprinkled points to have as many of the statistical properties of the Poisson point process (PPP) as possible. To that end, along with matching the (nearest neighbor) distance distribution of the PPP (see Appendix D), we also match the scaling of the maximal coordinate in deterministic sprinkling, x_n , with the scaling of the mean of the extreme value distribution of $U([0, 1])$ [67] by shifting the regular lattice, $u_i = (i - z)/n$ horizontally by $z = 1/2$.

To show this formally, let us consider n i.i.d. uniform random variables, i.e., $\xi_i \sim U([0, 1])$ and let $\xi_{\max} = \max(\xi_1, \xi_2, \dots, \xi_n)$. The cumulative distribution function of the maximal value is,

$$\mathbb{P}(\xi_{\max} \leq \xi) = \prod_{i=1}^n \mathbb{P}(\xi_i \leq \xi) = \xi^n. \quad (\text{C2})$$

This then allows us to derive the expected maximal value as,

$$\overline{\xi_{\max}} = n \int_0^1 \xi^n d\xi = \frac{n}{n+1} = 1 - \frac{1}{n} + \mathcal{O}\left(\frac{1}{n^2}\right). \quad (\text{C3})$$

In order for our deterministic process to give the same result, we must set z in $u_i = (i - z)/n$ appropriately such that $x_{\max} = x_n = 1 - 1/n$. From Eq. (C1) it is easy to see that $x_n = -1/n \sum_{i=1}^n \ln(1 - u_i)$, where the pseudo random permutation function, $\sigma(i)$, is irrelevant. The question now is how to choose $z \in [0, 1]$ such that the correct scaling is achieved. For some general value of z ,

$$\begin{aligned} x_n &= -\frac{1}{n} \sum_{i=1}^n \ln \left(1 - \frac{i - z}{n} \right), \\ &= -\frac{1}{n} \ln \left(\prod_{i=0}^{n-1} (i + z) \right) + \ln n, \\ &= -\frac{1}{n} \ln \left(\frac{\Gamma(z + n)}{\Gamma(z)} \right) + \ln n. \end{aligned} \quad (\text{C4})$$

The transcendental equation $x_n = \overline{\xi_{\max}}$ cannot be solved analytically, and we must therefore turn to asymptotics. In the setting $n \gg 1$, we can use the following,

$$\ln(\Gamma(w)) = \frac{2w-1}{2} \ln(w) - w + \frac{1}{2} \ln(2\pi) + \mathcal{O}\left(\frac{1}{w}\right), \quad (\text{C5})$$

to obtain,

$$x_n = 1 + \frac{1-2z}{2} \frac{\ln n}{n} + \frac{1}{n} \ln\left(\frac{\Gamma(z)}{\sqrt{2\pi}}\right) + \mathcal{O}\left(\frac{1}{n^2}\right). \quad (\text{C6})$$

The term of order $\mathcal{O}(\ln n/n)$ is not present in $\overline{\xi_{\max}}$. Therefore, it must be removed by setting $z = 1/2$, leading to

$$x_n = 1 - \frac{\ln 2}{2} \frac{1}{n} + \mathcal{O}\left(\frac{1}{n^2}\right). \quad (\text{C7})$$

This is not exactly the same expression as Eq. C3, but the constant pre-factor in the second term has no effect on the scaling behavior, so, for instance, the scaling of the largest hidden degree is $\kappa_{\max} \sim n^{1/(\gamma-1)}$ in both the random and derandomized cases.

Appendix D: Poisson point process, derandomized

In this section, we show that the hypercanonical derandomization in Sec. III B results in a deterministic sprinkling of n points on the unit interval and unit square matching the (nearest neighbor) distance distribution of the Poisson point process (PPP).

The nearest neighbor distance distribution in 1d and 2d PPP of intensity n is [39]

$$\begin{aligned} \mathbb{P}_{1d}^{(nn)}(x) &= 2ne^{-2nx}, \\ \mathbb{P}_{2d}^{(nn)}(x) &= 2\pi nxe^{-\pi nx^2}. \end{aligned} \quad (\text{D1})$$

The PPP distance distribution, on the other hand, is the probability density function of the distance between two random points on the unit interval, $\mathbb{P}_{1d}(x)$, or unit square, $\mathbb{P}_{2d}(x)$. It is given by [68]

$$\begin{aligned} \mathbb{P}_{1d}(x) &= \begin{cases} 2(1-x), & 0 \leq x \leq 1, \\ 0, & \text{otherwise;} \end{cases} \\ \mathbb{P}_{2d}(x) &= \begin{cases} 2x(\pi - 4x + x^2), & 0 \leq x \leq 1, \\ 2x[4\sqrt{x^2-1} - (x^2+2-\pi) - 4\arctan\sqrt{x^2-1}], & 1 < x \leq \sqrt{2}, \\ 0, & \text{otherwise.} \end{cases} \end{aligned} \quad (\text{D2})$$

In Fig. 5(a,b), we show a realization of the 2d PPP, and compare it with our deterministic process. In addition to pleasing visual similarity between the two observed there, Figs. 5(c,d) and Figs. 5(e,f) confirm that the deterministic sprinkling has the same (nearest neighbor) distance distribution as the PPP.

Appendix E: Random hyperbolic graphs (RHGs)

An important random graph model belonging to the class of HVNMs (Appendix B) is the degree-corrected latent space model, also known as random hyperbolic graphs (RHG) [40], which combines the properties of the hypersoft configuration model [62] and soft random geometric graphs [64, 65]. Here, we describe the \mathbb{H}^2 and \mathbb{S}^1 equivalent versions of this hypercanonical model [40, 41, 69].

In the \mathbb{H}^2 formulation, sampling a network first involves sprinkling nodes quasi-uniformly within a disk of radius $R_{\mathbb{H}^2}$ on the hyperbolic plane of constant curva-

ture $K = -1$. That is, the hidden variables of nodes i are their polar coordinates (r_i, θ_i) which are sampled independently as $\theta_i \sim U([0, 2\pi])$ and $r_i \sim \rho$, where the support of the radial coordinate distribution ρ is $[0, R_{\mathbb{H}^2}]$, and its PDF is

$$\rho(r) = \tilde{\alpha} \frac{\sinh(\tilde{\alpha}r)}{\cosh(\tilde{\alpha}R_{\mathbb{H}^2}) - 1}. \quad (\text{E1})$$

The parameter $\tilde{\alpha} \geq 1/2$ controls the power law exponent of the resulting degree distribution in the model via $\gamma = 2\tilde{\alpha} + 1$, while the radius of the disk

$$R_{\mathbb{H}^2} = 2 \ln \left(\frac{2n}{\bar{k}\beta} \csc\left(\frac{\pi}{\beta}\right) \left(\frac{\tilde{\alpha}}{\tilde{\alpha} - 1/2}\right)^2 \right), \quad (\text{E2})$$

fixes the average degree to $\bar{k} > 0$ at $n \rightarrow \infty$. The parameter $\beta > 1$, the inverse temperature, controls the average clustering in the model.

Upon the assignment of the coordinates, two nodes are connected with the grand canonical Fermi-Dirac connec-

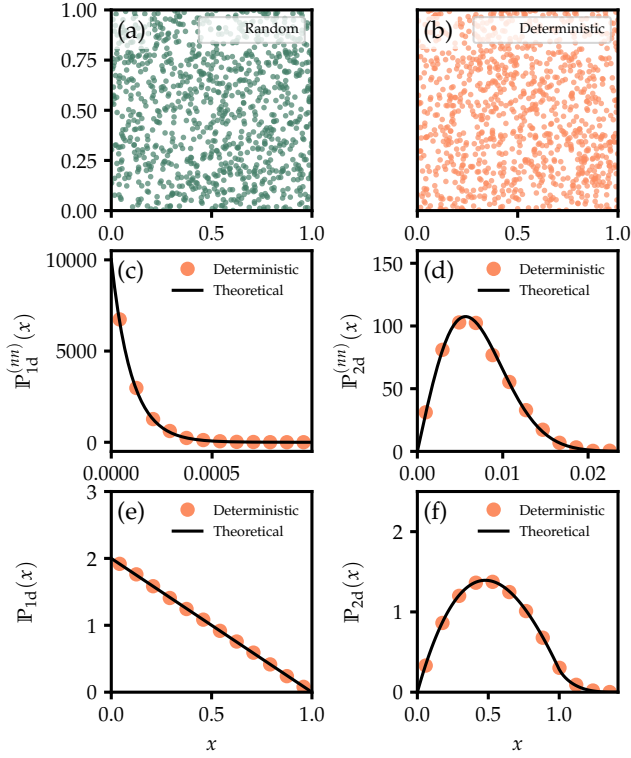


FIG. 5. **Poisson point process versus its derandomization.** (a) A realization of the PPP of intensity $n = 10^3$ on the unit square $[0, 1]^2$. (b) The deterministic sprinkling process from Sec. III B with $n = 10^3$. (c,d) The PPP nearest neighbor distance distributions in Eq. (D1), versus the empirical nearest neighbor distance distribution in the deterministic sprinkling process with $n = 5 \times 10^3$ on the unit interval and unit square, respectively. (e,f) The PPP distance distributions in Eq. (D2), versus the empirical distance distribution in the deterministic sprinkling with $n = 5 \times 10^3$ on the unit interval and unit square, respectively.

tion probability,

$$p_{ij} = \frac{1}{1 + e^{\beta(\tilde{\varepsilon}_{ij} - R_{\mathbb{H}^2})/2}}. \quad (\text{E3})$$

The fermionic energies $\tilde{\varepsilon}_{ij}$ are the hyperbolic distances between nodes i and j given by the hyperbolic law of cosines,

$$\cosh \tilde{\varepsilon}_{ij} = \cosh r_i \cosh r_j - \sinh r_i \sinh r_j \cos \Delta\theta_{ij}, \quad (\text{E4})$$

where $\Delta\theta_{ij} = \pi - |\pi - |\theta_i - \theta_j||$ is the angle between the two points. This distance is approximately equal to [40, 69]

$$\tilde{\varepsilon}_{ij} \approx r_i + r_j + 2 \ln \left(\frac{\Delta\theta_{ij}}{2} \right). \quad (\text{E5})$$

The \mathbb{H}^2 model is a hypercanonical mixture of the grand canonical models (Appendix A) with random link energies $\tilde{\varepsilon}_{ij}$ defined in Eq. (E5). Their distribution is the

distance distribution between random points on the hyperbolic disk.

In the equivalent \mathbb{S}^1 formulation of RHGs [40], each node is endowed with two random hidden variables: similarity (x_i) and popularity (κ_i). The similarity space is a circle of radius $R_{\mathbb{S}^1} = n/2\pi$ and $x_i = R_{\mathbb{S}^1}\theta_i$, where $\theta_i \sim U([0, 2\pi])$ (two nodes close on the circle are “similar”). The radius scales with n so as to maintain the node density on the circle to be one. The popularity hidden variables of nodes are their expected degrees $\kappa_i \sim \rho(\kappa|\bar{\kappa}, \gamma)$, where

$$\rho(\kappa|\bar{\kappa}, \gamma) = (\gamma - 1)\bar{\kappa}_0^{\gamma-1}\kappa^{-\gamma}, \quad (\text{E6})$$

is the Pareto distribution with mean $\bar{\kappa}$, power-law exponent γ , and support $\kappa \in [\kappa_0, \infty)$, where $\kappa_0 = \bar{\kappa}(\gamma - 2)/(\gamma - 1)$.

Once the hidden variables are assigned, two nodes are connected with the grand canonical Fermi-Dirac connection probability,

$$p_{ij} = \frac{1}{1 + \left(\frac{d_{ij}}{\hat{\mu}\kappa_i\kappa_j} \right)^\beta} = \frac{1}{1 + e^{\beta(\varepsilon_{ij} - \mu)}}, \quad \text{where} \quad (\text{E7})$$

$$d_{ij} = R_{\mathbb{S}^1} \Delta\theta_{ij}, \quad \mu = \log(\hat{\mu}), \quad \text{and}$$

$$\varepsilon_{ij} = \log \left(\frac{d_{ij}}{\kappa_i\kappa_j} \right)$$

are the link energies in the model. The inverse temperature $\beta > 1$ is the same as in the \mathbb{H}^2 formulation, while the chemical potential

$$\hat{\mu} = \frac{\beta}{2\pi\bar{\kappa}} \sin \left(\frac{\pi}{\beta} \right) \quad (\text{E8})$$

fixes the expected average degree in the model to $\bar{\kappa} > 0$ at $n \rightarrow \infty$. For completeness, we re-derive this observation in Appendix F.

The \mathbb{H}^2 and \mathbb{S}^1 formulations of RHGs are equivalent because they have the same distributions of hidden variables and connection probabilities. Indeed, the angular coordinates in both formulations come from the same uniform distribution, while the radial coordinate and expected degree distributions $\rho(r)$ and $\rho(\kappa)$ in Eqs. (E1, E6) can be obtained from each other via the following change of variables:

$$\kappa = \kappa_0 e^{(R_{\mathbb{H}^2} - r)/2}, \quad (\text{E9})$$

which maps the connection probability in Eq. (E7) to the one in Eq. (E3) [40].

This change of variables leads to the following relationship between the link energies in the two formulations:

$$\tilde{\varepsilon}_{ij} = 2 \left[\varepsilon_{ij} + \ln \left(\frac{n}{\tau} \right) \right], \quad (\text{E10})$$

where $\tau = \pi\kappa_0^2\hat{\mu}^2$. Consequently, the graph energy and expected energy are related via

$$\begin{aligned} \tilde{\varepsilon}(G) &= 2 \left[\varepsilon(G) + \ln \left(\frac{n}{\tau} \right) m(G) \right], \\ \bar{\tilde{\varepsilon}} &= 2 \left[\bar{\varepsilon} + \ln \left(\frac{n}{\tau} \right) \bar{m} \right]. \end{aligned} \quad (\text{E11})$$

All the analytical and simulation results reported in this paper are obtained using the \mathbb{S}^1 formulation of the RHG model since it is easier to work with. In particular, to simulate RHGs, we take their size n and parameters $\bar{\kappa} > 0$, $\beta > 1$, and $\gamma > 2$ as input, and proceed as described the second half of this section.

Appendix F: Self-averaging of RHGs' sufficient statistics

In this section, we derive the closed-form expressions for the mean values of the number of links $m(G) = \sum_{i < j} G_{ij}$, and energy $\varepsilon(G) = \sum_{i < j} \varepsilon_{ij} G_{ij}$ of the random hyperbolic graphs (Appendix E) in the thermodynamic limit $n \rightarrow \infty$. We also show that the distributions of these random variables are self-averaging—their coefficient of variation goes to zero in the thermodynamic limit for any value of the degree exponent $\gamma > 2$.

1. Average number of links (\bar{m})

The average number of links in the model is,

$$\begin{aligned} \bar{m} &= \mathbb{E} \left[\sum_{i < j} G_{ij} \right], \\ &= \binom{n}{2} \mathbb{E}[G_{ij}], \\ &= \frac{1}{2} \int_{-n/2}^{n/2} \int_{\kappa_0}^{\infty} m(\kappa_i, x_i) \rho(\kappa_i) dx_i d\kappa_i, \end{aligned}$$

where $m(\kappa_i, x_i) = (n-1) \int_{-n/2}^{n/2} \int_{\kappa_0}^{\infty} p_{ij} \frac{\rho(\kappa_j)}{n} dx_j d\kappa_j$. (F1)

$m(\kappa_i, x_i)$ is the expected number of links attached to node “ i ” with hidden variable values (κ_i, x_i) . Due to the model being rotationally invariant, we can set $x_i = 0$ without loss of generality, i.e., $m(\kappa_i, 0) = m(\kappa_i, x_i)$, which in the limit $n \rightarrow \infty$ is,

$$\begin{aligned} m(\kappa_i, 0) &= 2 \int_0^{\infty} \int_{\kappa_0}^{\infty} \frac{1}{1 + \left(\frac{x_j}{\hat{\mu} \kappa_i \kappa_j} \right)^{\beta}} \rho(\kappa_j) dx_j d\kappa_j, \\ &= 2 \hat{\mu} \kappa_i \bar{\kappa} \frac{\pi}{\beta} \csc \left(\frac{\pi}{\beta} \right). \end{aligned} \quad (F2)$$

Hence, the average number of links in the model is,

$$\begin{aligned} \bar{m} &= \frac{n}{2} \int_{\kappa_0}^{\infty} m(\kappa_i, 0) \rho(\kappa_i) d\kappa_i, \\ &= n \hat{\mu} \bar{\kappa}^2 \frac{\pi}{\beta} \csc \left(\frac{\pi}{\beta} \right). \end{aligned} \quad (F3)$$

By requiring that $\bar{\kappa} = \bar{k} = 2\bar{m}/n$ in the last equation, we get the expression for the chemical potential in Eq. (E8).

2. Average energy ($\bar{\varepsilon}$)

Similarly, the average energy of the model is,

$$\begin{aligned} \bar{\varepsilon} &= \mathbb{E} \left[\sum_{i < j} G_{ij} \varepsilon_{ij} \right], \\ &= \binom{n}{2} \mathbb{E}[G_{ij} \varepsilon_{ij}], \\ &= \frac{1}{2} \int_{-n/2}^{n/2} \int_{\kappa_0}^{\infty} \varepsilon(\kappa_i, x_i) \rho(\kappa_i) dx_i d\kappa_i, \end{aligned}$$

$$\text{where } \varepsilon(x_i, \kappa_i) = (n-1) \int_{-n/2}^{n/2} \int_{\kappa_0}^{\infty} p_{ij} \varepsilon_{ij} \frac{\rho(\kappa_j)}{n} dx_j d\kappa_j. \quad (F4)$$

Once again, due to the model being rotationally invariant, we set $x_i = 0$ without loss of generality, i.e., $\varepsilon(\kappa_i, x_i) = \varepsilon(\kappa_i, 0)$, which in the $n \rightarrow \infty$ limit results in,

$$\begin{aligned} \varepsilon(\kappa_i, 0) &= 2 \int_0^{\infty} \int_{\kappa_0}^{\infty} \frac{\log \left(\frac{x_j}{\kappa_i \kappa_j} \right)}{1 + \left(\frac{x_j}{\hat{\mu} \kappa_i \kappa_j} \right)^{\beta}} \rho(\kappa_j) d\kappa_j dx_j, \\ &= 2 \hat{\mu} \kappa_i \bar{\kappa} \csc \left(\frac{\pi}{\beta} \right) \frac{\pi}{\beta^2} \left(\beta \log(\hat{\mu}) - \pi \cot \left(\frac{\pi}{\beta} \right) \right). \end{aligned} \quad (F5)$$

Finally,

$$\begin{aligned} \bar{\varepsilon} &= \frac{n}{2} \int_{\kappa_0}^{\infty} \varepsilon(0, \kappa_i) \rho(\kappa_i) d\kappa_i, \\ &= n \hat{\mu} (\bar{\kappa})^2 \csc \left(\frac{\pi}{\beta} \right) \frac{\pi}{\beta^2} \left(\beta \log(\hat{\mu}) - \pi \cot \left(\frac{\pi}{\beta} \right) \right), \quad (F6) \\ &= \frac{n}{2} \bar{\kappa} \left(\log \left(\frac{\beta \sin \left(\frac{\pi}{\beta} \right)}{2\pi \bar{\kappa}} \right) - \frac{\pi}{\beta} \cot \left(\frac{\pi}{\beta} \right) \right), \end{aligned}$$

where in the last step, we have used the expression for the chemical potential in Eq. (E8).

3. Asymptotics of the coefficients of variation of m and ε

To prove that the distribution of the number of links, $m(G)$ and energy, $\varepsilon(G)$ of the \mathbb{S}^1 model is self-averaging, we need to show that their respective coefficients of variation $C_V^{(m)}(n) = \sqrt{\text{Var}(m)}/\mathbb{E}[m]$ and $C_V^{(\varepsilon)}(n) = \sqrt{\text{Var}(\varepsilon)}/\mathbb{E}[\varepsilon]$ go to zero in the limit $n \rightarrow \infty$. In Sec. F1 and Sec. F2 we have already calculated the expected values of the number of links and energy, showing that \bar{m} and $\bar{\varepsilon}$ both scale as $\mathcal{O}(n)$, for some fixed value of $\bar{\kappa}$. We next need to find the variance of the random variables $m(G)$ and $\varepsilon(G)$.

The variance of the number of links is,

$$\text{Var}[m] = \sum_{i < j} \text{Var}[G_{ij}] + 2 \sum_{(i,j) < (k,l)} \text{Cov}[G_{ij}, G_{kl}]. \quad (F7)$$

The first term scales as,

$$\begin{aligned} \sum_{i < j} \text{Var}[G_{ij}] &= \binom{n}{2} (\mathbb{E}[G_{ij}^2] - \mathbb{E}[G_{ij}]^2) \\ &= C_1 n \cdot (1 + o(1)), \\ \text{where } C_1 &= \hat{\mu} \bar{\kappa}^2 \frac{\pi}{\beta} \csc\left(\frac{\pi}{\beta}\right), \end{aligned} \quad (\text{F8})$$

since $\mathbb{E}[G_{ij}^2] = \mathbb{E}[G_{ij}] = \mathcal{O}(n^{-1})$. To obtain the scaling of the second term, we first point out that non-zero contributions to the sum come from covariance between two edge indicators that share a common node, $\text{Cov}[G_{ij}, G_{ik}]$, i.e., *wedges* (\blacktriangle). The covariance terms that do not share a common node, $\text{Cov}[G_{ij}, G_{kl}]$, i.e. ($\bullet\bullet$), are simply zero because G_{ij} and G_{kl} are independent random variables. To that end,

$$\begin{aligned} 2 \sum_{(i,j) < (k,l)} \text{Cov}[G_{ij}, G_{kl}] &= 6 \binom{n}{3} \text{Cov}[G_{ij}, G_{ik}], \\ &= n^3 \text{Cov}[G_{ij}, G_{ik}] \cdot (1 + o(1)), \\ \text{where } \text{Cov}[G_{ij}, G_{ik}] &= \mathbb{E}[G_{ij} G_{ik}] - \mathbb{E}[G_{ij}] \mathbb{E}[G_{ik}]. \end{aligned} \quad (\text{F9})$$

Once we get the asymptotics of the term $\mathbb{E}[G_{ij} G_{ik}]$ we are done, since $\mathbb{E}[G_{ij}] \mathbb{E}[G_{ik}] = (4C_1^2/n^2) \cdot (1 + o(1))$. Notice that from the tower rule we have,

$$\begin{aligned} \mathbb{E}[G_{ij} G_{ik}] &= \mathbb{E}_{\kappa_i, x_i} [\mathbb{E}[G_{ij} G_{ik} | \kappa_i, x_i]], \\ &= \mathbb{E}_{\kappa_i, x_i} [\mathbb{E}[G_{ij} | \kappa_i, x_i] \cdot \mathbb{E}[G_{ik} | \kappa_i, x_i]], \\ &= \mathbb{E}_{\kappa_i, x_i} [\Phi(\kappa_i, x_i)^2], \\ \text{where } \Phi(\kappa_i, x_i) &= \int_{-n/2}^{n/2} \int_{\kappa_0}^{\infty} p_{ij} \frac{\rho(\kappa_j)}{n} dx_j d\kappa_j. \end{aligned} \quad (\text{F10})$$

Once again using the fact that the model is rotationally invariant, we set $x_i = 0$ without loss of generality, i.e., $\Phi(\kappa_i, x_i) = \Phi(\kappa_i, 0)$. For $n \gg 1$, we get,

$$\Phi(\kappa_i, 0) = \frac{2\hat{\mu}\kappa_i\bar{\kappa}}{n} \frac{\pi}{\beta} \csc\left(\frac{\pi}{\beta}\right). \quad (\text{F11})$$

Further,

$$\begin{aligned} \mathbb{E}[G_{ij} G_{ik}] &= \mathbb{E}_{\kappa_i, x_i} [\Phi(\kappa_i, 0)^2], \\ &= \int_{\kappa_0}^{\infty} \left(\frac{2\hat{\mu}\kappa_i\bar{\kappa}}{n} \frac{\pi}{\beta} \csc\left(\frac{\pi}{\beta}\right) \right)^2 \rho(\kappa_i) d\kappa_i, \\ &= C_2 \frac{\bar{\kappa}^2}{n^2}, \\ \text{where } C_2 &= \left(\frac{2\hat{\mu}\bar{\kappa}\pi}{\beta} \csc\left(\frac{\pi}{\beta}\right) \right)^2. \end{aligned} \quad (\text{F12})$$

Combining these results and plugging them back into Eq. (F7),

$$\text{Var}[m] = C_1 (1 - 4C_1) n + C_2 \bar{\kappa}^2 n. \quad (\text{F13})$$

For any $\gamma > 2$, the first moment of the Pareto distribution is $\bar{\kappa} = \mathcal{O}(1)$ but the second moment scales as,

$$\begin{aligned} \bar{\kappa}^2 &= \int_{\kappa_0}^{\kappa_0 n^{\frac{1}{\gamma-1}}} \kappa^2 \rho(\kappa) d\kappa \\ &= \begin{cases} \frac{\gamma-1}{3-\gamma} \kappa_0^2 n^{\frac{3-\gamma}{\gamma-1}}, & 2 < \gamma < 3, \\ \kappa_0^2 \ln n, & \gamma = 3, \\ \frac{\gamma-1}{\gamma-3} \kappa_0^2, & \gamma > 3. \end{cases} \end{aligned} \quad (\text{F14})$$

Hence, depending on the value of $\gamma > 2$, the scaling of the coefficients of variation of the distribution of the number of links, $C_V^{(m)}(n) = \sqrt{\text{Var}(m)}/\mathbb{E}[m]$, in the \mathbb{S}^1 model is given by,

$$C_V^{(m)}(n) = \begin{cases} \frac{\sqrt{C_2(\gamma-1)/(3-\gamma)} \kappa_0}{C_1} n^{-\frac{\gamma-2}{\gamma-1}} \cdot (1 + o(1)), & 2 < \gamma < 3, \\ \frac{\sqrt{C_2} \kappa_0}{C_1} \sqrt{\frac{\ln(n)}{n}} \cdot (1 + o(1)), & \gamma = 3, \\ \frac{\sqrt{C_1(1-4C_1) + C_2\kappa_0^2(\gamma-1)/(\gamma-3)}}{C_1} \frac{1}{\sqrt{n}} \cdot (1 + o(1)), & \gamma > 3. \end{cases} \quad (\text{F15})$$

The same procedure above is repeated verbatim to derive the asymptotics of the variance of energy,

$$\begin{aligned} \text{Var}[\varepsilon] &= \sum_{i < j} \text{Var}[G_{ij} \varepsilon_{ij}] + 2 \sum_{(i,j) < (k,l)} \text{Cov}[G_{ij} \varepsilon_{ij}, G_{kl} \varepsilon_{kl}]. \end{aligned} \quad (\text{F16})$$

Consider the first term,

$$\sum_{i < j} \text{Var}[G_{ij} \varepsilon_{ij}] = \binom{n}{2} (\mathbb{E}[(G_{ij} \varepsilon_{ij})^2] - \mathbb{E}[G_{ij} \varepsilon_{ij}]^2). \quad (\text{F17})$$

The expression for $\mathbb{E}[G_{ij} \varepsilon_{ij}]$ is calculated in Sec. F2; on

the other hand,

$$\binom{n}{2} \mathbb{E}[(G_{ij}\varepsilon_{ij})^2] = \frac{1}{2} \int_{-n/2}^{n/2} \int_{\kappa_0}^{\infty} \varepsilon'(\kappa_i, x_i) \rho(\kappa_i) dx_i d\kappa_i,$$

where $\varepsilon'(x_i, \kappa_i) = (n-1) \int_{-n/2}^{n/2} \int_{\kappa_0}^{\infty} p_{ij} \varepsilon_{ij}^2 \frac{\rho(\kappa_j)}{n} dx_j d\kappa_j$.

(F18)

Once again, using the fact that the model is rotationally invariant, we set $x_i = 0$ without loss of generality, i.e., $\varepsilon'(x_i, \kappa_i) = \varepsilon'(0, \kappa_i)$, which in the $n \rightarrow \infty$ limit results in,

$$\begin{aligned} \varepsilon'(0, \kappa_i) &= 2 \int_0^{\infty} \int_{\kappa_0}^{\infty} \frac{\log^2 \left(\frac{x_j}{\kappa_i \kappa_j} \right)}{1 + \left(\frac{x_j}{\hat{\mu} \kappa_i \kappa_j} \right)^{\beta}} \rho(\kappa_j) d\kappa_j dx_j, \\ &= 2 \hat{\mu} \kappa_i \bar{\kappa} \frac{\pi}{\beta} \csc \left(\frac{\pi}{\beta} \right) \left[\left(\log(\hat{\mu}) - \frac{\pi}{\beta} \cot \left(\frac{\pi}{\beta} \right) \right)^2 \right. \\ &\quad \left. + \left(\frac{\pi}{\beta} \csc \left(\frac{\pi}{\beta} \right) \right)^2 \right] = \frac{2 \kappa_i C'_1}{\bar{\kappa}}. \end{aligned}$$

(F19)

Hence,

$$\binom{n}{2} \mathbb{E}[(G_{ij}\varepsilon_{ij})^2] = n C'_1 \cdot (1 + o(1)), \quad (F20)$$

which is the asymptotic scaling of the first term in Eq. (F16). Following a similar argument as in the previous case, the asymptotics of the second term in Eq. (F16) is,

$$\begin{aligned} 2 \sum_{(i,j) < (k,l)} \text{Cov}[G_{ij}\varepsilon_{ij}, G_{kl}\varepsilon_{kl}] &= n^3 (\mathbb{E}[G_{ij}\varepsilon_{ij} G_{ik}\varepsilon_{ik}] \\ &\quad - \mathbb{E}[G_{ij}\varepsilon_{ij}] \mathbb{E}[G_{ik}\varepsilon_{ik}]), \\ \text{where, } \mathbb{E}[G_{ij}\varepsilon_{ij}] \mathbb{E}[G_{ik}\varepsilon_{ik}] &= (C'_2/n^2) \cdot (1 + o(1)); \\ \left(\bar{\kappa} \log(\hat{\mu}) - \bar{\kappa} \frac{\pi}{\beta} \cot \left(\frac{\pi}{\beta} \right) \right)^2 &= C'_2. \end{aligned}$$

(F21)

Further,

$$\mathbb{E}[G_{ij}\varepsilon_{ij} G_{ik}\varepsilon_{ik}] = \mathbb{E}_{\kappa_i, x_i} [\Phi'(\kappa_i, x_i)^2],$$

where $\Phi'(\kappa_i, x_i) = \int_{-n/2}^{n/2} \int_{\kappa_0}^{\infty} p_{ij} \varepsilon_{ij} \frac{\rho(\kappa_j)}{n} dx_j d\kappa_j$.

(F22)

But $\Phi'(\kappa_i, x_i) = \Phi'(\kappa_i, 0)$, which in the setting $n \gg 1$ is,

$$\begin{aligned} \Phi'(\kappa_i, 0) &= \frac{2 \hat{\mu} \kappa_i}{n} \bar{\kappa} \csc \left(\frac{\pi}{\beta} \right) \frac{\pi}{\beta^2} \left(\beta \log(\hat{\mu}) - \pi \cot \left(\frac{\pi}{\beta} \right) \right), \\ &= \frac{\kappa_i \sqrt{C'_2}}{n \bar{\kappa}}, \end{aligned}$$

(F23)

leading to the result,

$$\begin{aligned} \mathbb{E}[G_{ij}\varepsilon_{ij} G_{ik}\varepsilon_{ik}] &= \int_{\kappa_0}^{\infty} \Phi'(\kappa_i, 0)^2 \rho(\kappa_i) d\kappa_i \\ &= C'_2 \frac{\bar{\kappa}^2}{\bar{\kappa}^2 n^2}. \end{aligned}$$

(F24)

Plugging all these results into Eq. (F16) we have,

$$\text{Var}[\varepsilon] = n (C'_1 - C'_2) + n C'_2 \frac{\bar{\kappa}^2}{\bar{\kappa}^2} \quad (F25)$$

Hence, depending on the value of $\gamma > 2$, the scaling of the coefficients of variation of the distribution of the energy, $C_V^{(\varepsilon)}(n) = \sqrt{\text{Var}(\varepsilon)}/\mathbb{E}[\varepsilon]$, in the \mathbb{S}^1 model is given by,

$$|C_V^{(\varepsilon)}(n)| = \begin{cases} \frac{2 \kappa_0}{\bar{\kappa}} \sqrt{\frac{\gamma-1}{3-\gamma}} n^{-\frac{\gamma-2}{\gamma-1}} \cdot (1 + o(1)), & 2 < \gamma < 3, \\ \frac{2 \kappa_0}{\bar{\kappa}} \sqrt{\frac{\ln(n)}{n}} \cdot (1 + o(1)), & \gamma = 3, \\ 2 \sqrt{\frac{(C'_1 - C'_2) + C'_2 \frac{\kappa_0^2 (\gamma-1)}{\bar{\kappa}^2 (\gamma-3)}}{C'_2}} \frac{1}{\sqrt{n}} \cdot (1 + o(1)), & \gamma > 3. \end{cases} \quad (F26)$$

We conclude that the coefficients of variation of both the distribution of the number of links and energy scale

as

$$C_V(n) = \mathcal{O} \left(n^{-\min\{\frac{1}{2}, \frac{\gamma-2}{\gamma-1}\}} (\ln(n))^{\frac{1}{2} \mathbb{1}_{\{\gamma=3\}}} \right) \quad (F27)$$

and hence are self-averaging distributions for any $\gamma > 2$ since $\lim_{n \rightarrow \infty} C_V(n) = 0$.

Appendix G: Deterministic hyperbolic graphs (DHGs)

In this section, we outline the exact details involved in the deterministic construction of typical networks in the random hyperbolic graph (RHG) model (Appendix E), which we call *deterministic hyperbolic graphs* (DHGs).

The input parameters are the same as in the RHG model: n , $\bar{\kappa}$, β , and γ . The rest is different. First, hidden variables, (κ_i, x_i) , are assigned to each node deterministically via the two-dimensional hypercanonical derandomization in Sec. III B. This derandomization returns deterministic coordinates $(\tilde{x}_i, \tilde{y}_i)$ on the unit square, which we then use to obtain the RHG hidden variables. We set the similarity space coordinate to $x_i = n\tilde{x}_i$, while the expected degree κ_i is obtained via the inverse CDF of the Pareto distribution applied to \tilde{y}_i :

$$\kappa_i = \bar{\kappa} \frac{\gamma - 2}{\gamma - 1} (1 - \tilde{y}_i)^{\frac{1}{1-\gamma}}. \quad (\text{G1})$$

Once the hidden variables are determined, the value of the chemical potential $\hat{\mu}$ in Eq. (E7) is obtained by finding the root of the equation

$$\sum_{i < j} p_{ij} - \frac{n\bar{\kappa}}{2} = 0 \quad (\text{G2})$$

numerically using Newton's method with analytically calculated derivative of the objective function and absolute tolerance of $\tau = 10^{-8}$. This ensures that the DHG exactly matches the desired value of one sufficient statistic, the number of edges $m^* = \lfloor n\bar{\kappa}/2 \rfloor$. Another option would be to use the analytical thermodynamic-limit expression for $\hat{\mu}$ in Eq. (E8), but the convergence of the number of edges m and energy ε of DHGs to the ensemble average of RHGs would be slower in this case. Another reason to avoid this option is that upon hypercanonical derandomization, we end up dealing with a unique single instance of the grand canonical ensemble, so we can use it to find the exact value of the chemical potential.

Finally, having this grand canonical ensemble in place, in which all the pairwise connection probabilities are now determined, we use the grand canonical derandomization procedure in Sec. III A to deterministically place all the m^* edges.

We make the software package implementing the described DHG construction procedure available at [43].

Appendix H: Real-world networks

1. Parameter estimation

To compare real-world networks with the corresponding most typical networks in the deterministic hyperbolic

graph (DHG) model, we first have to measure the value of the model parameters—the numbers of nodes n and links m , the degree distribution exponent γ , and the inverse temperature β —in the real-world networks. We do this as follows.

Determining the number of nodes and links is trivial. To measure the degree distribution exponent, we follow the prescription in [70]. We employ the **tail-estimation** software package [71], and use three different estimators of the extreme value exponent ξ , which is related to the degree exponent by $\gamma = 1 + 1/\xi$. These estimators are the Kernel estimator $\hat{\gamma}_K$, Hill estimator $\hat{\gamma}_H$, and Moment estimator $\hat{\gamma}_M$. We use the value of γ determined with the Moments estimator to construct networks in the DHG model.

To determine the inverse temperature β for fixed values of n , m , and γ , we first compute the average clustering in a real-world network, excluding nodes of degrees < 2 :

$$\bar{c} = \frac{1}{|V_{k \geq 2}|} \sum_{i \in V_{k \geq 2}} c_i, \quad (\text{H1})$$

where $V_{k \geq 2} = \{i \in V : k_i \geq 2\}$ is the set of nodes with degree k at least two, $c_i = t_i / \binom{k_i}{2}$ is the clustering coefficient of node i , k_i is its degree, and t_i is the number of triangles it is in. Since the DHG is a deterministic model it generates a single graph with a fixed value of average clustering $\bar{c}_{\text{DHG}}(n, m, \gamma, \beta)$ for any combination of its parameters. We then use Brent's method [72], as implemented in SciPy [73] (v1.16.1) to find the root β^* of

$$f(\beta) = \bar{c} - \bar{c}_{\text{DHG}}(n, \bar{k}, \gamma, \beta) \quad (\text{H2})$$

in the interval $[1, 10]$ and treat it as an estimate $\hat{\beta} = \beta^*$ of the inverse temperature. Since clustering is an increasing function of β , if we do not find a root in this interval and the empirical clustering is larger than the clustering in the model at $\beta = 10$, we set $\hat{\beta} = 10$. If we do not find a root in the interval and the empirical clustering is lower than the clustering in the model for $\beta = 1$, we set $\hat{\beta} = 1$.

2. Network data and network properties

We infer the parameters discussed in the previous section for seventeen networks in the **Netzschleuder** network repository [74], which contains a variety of real-world networks from different domains, including social networks, biological networks, transportation networks, technological networks, and literature/word networks. For each network, as soon as its parameters are inferred, we also construct the unique DHG network with the same parameter values, using the code available at [43].

In the resulting seventeen pairs of real-world and DHG networks, we then measure the following network properties:

- distribution $\mathbb{P}(k)$ of node degrees k , and the average degree $\bar{k} = \sum_k kP(k) = 2m/n$;
- average local clustering coefficient $c(k)$ of $(k > 1)$ -degree nodes, and the average clustering $\bar{c} = \sum_{k>1} c(k)P(k)$;
- average degree $k_{nn}(k)$ of neighbors of k -degree nodes, and the Spearman correlation coefficient ρ of degrees of connected nodes;
- distribution $\mathbb{P}(d)$ of shortest path distances d between all pairs of nodes, and the average distance $\bar{d} = \sum_d dP(d)$;
- average betweenness centrality $b(k)$ of k -degree nodes;
- distribution $\mathbb{P}(n_{cn})$ of the number of common neighbors n_{cn} of all pairs of connected nodes, also known as edge multiplicity [44]; and
- fraction ν^{lcc} of nodes in the largest connected component.

3. Network visualization

We also develop an algorithm inspired by LaNet-vi [75–77] to visualize the largest connected component of all networks. Note, that all quantities in this section are computed after subsetting a given network to its largest connected component. The visualization algorithm assigns a radial r_i and angular $\varphi_i \in [0, 2\pi)$ coordinate to each node i as follows.

First, we determine the coreness u_i of node i in the k -core decomposition. We encode this value using the color [78] of a vertex. Nodes of the same value of coreness u form a shell $Q_u = \{i \in V : u_i = u\}$. We also compute the adjusted coreness u'_i of node i as a convex combination of its own coreness u_i and the coreness of its neighbors,

$$u'_i = \varepsilon u_i + (1 - \varepsilon) \frac{1}{k_i} \sum_{j \in V} G_{ij} u_j, \quad (\text{H3})$$

where k_i is the degree of node i , G_{ij} the adjacency matrix, and $\varepsilon \in [0, 1]$ a parameter of the algorithm that governs the relative influence of a nodes' coreness u_i and the average coreness of its neighbors on the adjusted coreness. We set $\varepsilon = 0.85$ for our visualization.

The radial coordinate r_i of node i is then

$$r_i = (r_1 - r_0) \frac{u'_{\max} - u'_i}{u'_{\max} - u'_{\min}} + r_0, \quad (\text{H4})$$

where $r_1 \geq r_0 > 0$ are constants governing the maximum and minimum radial coordinate in the visualization, and $u'_{\min} = \min\{u'_i : i \in V\}$ and $u'_{\max} = \max\{u'_i : i \in V\}$ are smallest and largest values of adjusted coreness.

The angular coordinate φ_i of node i is determined by constructing the node-induced subgraphs $S_u = (Q_u, (Q_u \times Q_u) \cap E)$ of a given shell Q_u . We denote the N_u connected components of S_u as $C_{u,j}$ where $j \in \{1, 2, \dots, N_u\}$ enumerate them in arbitrary order. Each connected component $C_{u,j}$ is then assigned an angular segment $\Phi_{u,j}$ of arc length proportional to their relative size:

$$\Phi_{u,j} = \left[\sum_{i=1}^{j-1} \frac{2\pi}{N_u} \frac{|C_{u,i}|}{|Q_u|}, \sum_{i=1}^j \frac{2\pi}{N_u} \frac{|C_{u,i}|}{|Q_u|} \right). \quad (\text{H5})$$

Finally, the angular coordinate φ_i of node i belonging to connected component C_{u,j_i} is chosen uniformly at random in $\Phi_{u,j}$, i.e., $\varphi_i \sim U[\Phi_{u,j_i}]$.

All nodes also have sizes s_i , which grows with the logarithm of their degree k_i :

$$s_i = (s_1 - s_0) + \frac{\log k_i - \log k_{\min}}{\log k_{\max} - \log k_{\min}} + s_0 \quad (\text{H6})$$

where $s_1 \geq s_0 > 0$ are constants that govern the maximum and minimum node size respectively, and k_{\max}, k_{\min} are the maximum and minimum degree.

We only show a subset of all edges. Depending on network size and density we randomly select a subset of edges. Our visualizations retain between 0.25% and 100% of edges.

We make the code implementing the described graph visualization procedure available at [79].

4. Real-world networks vs. their DHG counterparts

Table I and Figures 6-19 present the results of the inferences, measurements, and visualizations described in the preceding sections for all the seventeen network pairs. In what follows, we provide some network-specific comments for each network pair.

a. Social Networks

The **inplod** network [80] (Fig. 6) represents the Turkish online Q&A platform. Nodes are users, and edges between nodes indicate that at least one of the two users follows the other. The DHG model (orange circles) with matched parameters is able to reproduce the broad degree distribution (panel (a)), clustering (panel (c)) small worldness (panel (e)) of the real-world network (blue squares). However, the model only qualitatively captures disassortativity (panel (b)) overestimates betweenness centrality (panel (f)), has a less broad distribution of common neighbors (panel (g)). We provide artistic visualizations of the real-world network (panel (d)) and its deterministic counterpart (panel (h)), showing 0.35% of edges.

In the **cora** citation network [81] (Fig. 7) nodes are scientific publications and edges encode that one paper

name	n	\bar{k}_{det}	\bar{k}_{real}	$\hat{\gamma}_{\text{H}}$	$\hat{\gamma}_{\text{M}}$	$\hat{\gamma}_{\text{K}}$	$\hat{\beta}$	\bar{c}_{det}	\bar{c}_{real}	\bar{d}_{det}	\bar{d}_{real}	$\nu_{\text{det}}^{\text{lcc}}$	$\nu_{\text{real}}^{\text{lcc}}$	ρ_{det}	ρ_{real}	domain
inplod [80]	39749	2.49	2.49	2.47	2.52	2.40	2.05	0.43	0.43	3.38	5.19	0.36	0.66	-0.29	0.02	social
cora [81]	23166	7.70	7.70	3.31	3.44	3.57	1.82	0.31	0.31	5.86	6.35	1.00	1.00	0.18	0.09	social
anybeat [82]	12645	7.77	7.77	2.37	2.49	2.54	1.72	0.40	0.40	3.17	3.63	1.00	0.99	-0.31	-0.04	social
bitcoin_trust [83]	5881	7.31	7.31	2.50	2.80	2.24	1.60	0.29	0.29	3.57	4.19	1.00	1.00	-0.13	-0.00	social
linux [84]	30837	13.83	13.83	2.60	2.03	1.95	1.00	0.14	0.31	3.25	2.82	1.00	1.00	-0.02	-0.27	technological
internet_as [85]	22963	4.22	4.22	2.09	2.10	2.13	1.20	0.35	0.35	3.84	3.47	1.00	0.83	0.14	-0.26	technological
google [86]	15763	18.85	18.85	2.52	2.34	2.15	2.24	0.60	0.60	2.52	2.73	1.00	1.00	-0.09	-0.11	technological
jdk [84]	6434	16.68	16.68	2.28	2.22	2.13	2.39	0.68	0.68	2.12	2.50	1.00	1.00	-0.25	-0.19	technological
interactome_figeys [87]	2239	5.75	5.75	2.45	2.38	2.43	1.00	0.07	0.09	3.84	3.84	0.99	0.99	-0.01	-0.06	biological
celegans_metabolic [88]	453	8.94	8.94	2.55	2.45	2.59	2.69	0.66	0.65	2.66	2.60	1.00	0.99	-0.20	-0.17	biological
celegans_neural [2, 89]	297	14.46	14.46	3.36	4.08	7.54	1.73	0.31	0.31	2.45	2.61	1.00	1.00	-0.11	0.09	biological
marvel_universe [90]	19428	9.83	9.83	2.55	2.27	2.14	1.00	0.00	0.10	4.45	3.42	0.99	1.00	-0.03	-0.08	literary
bible_nouns [74]	1773	10.30	10.30	3.04	3.30	2.91	6.57	0.72	0.72	3.37	4.52	0.96	1.00	0.37	0.14	literary
game_thrones [91]	107	6.58	6.58	4.01	3.08	3.20	3.97	0.65	0.65	2.88	2.69	1.00	0.99	0.09	0.04	literary
faa_routes [74]	1226	3.93	3.93	3.79	12.09	7.35	1.16	0.07	0.07	5.92	6.25	1.00	1.00	0.04	0.10	transport
euroroad [92]	1174	2.41	2.41	6.50	23.86	-	1.00	0.02	0.03	18.35	9.93	0.89	0.94	0.23	0.02	transport
london_transport [93]	369	2.33	2.33	4.17	4.60	1.00	1.00	0.03	0.04	13.70	7.42	1.00	0.89	0.19	0.04	transport

TABLE I. **Basic network properties of real-world versus DHG networks.** The table displays the measured values of the deterministic hyperbolic graph (DHG) parameters (Section H1)—number of nodes n , average degree \bar{k} , inverse temperature estimate $\hat{\beta}$, and degree distribution exponent $\hat{\gamma}_{\text{M}}$ estimated by the Moments estimator—for the seventeen real-world networks from the *Netzschleuder* network repository (Section H2). The table also reports the values of the degree distribution exponent estimated by the the Kernel $\hat{\gamma}_{\text{K}}$ and Hill $\hat{\gamma}_{\text{H}}$ estimators, and juxtaposes the real-world (subscript “real”) and DHG (subscript “det”) networks in terms of average local clustering \bar{c} , average shortest path length \bar{d} , fraction of nodes in the largest connected component ν^{lcc} , and the Spearman correlation coefficient ρ of the degrees of connected nodes.

cites the other. The DHG model (orange circles) accurately describes many properties of the real-world network (blue squares). This includes the degree distribution (panel (a)), assortativity (panel (b)) clustering (panel (c)), pairwise distance distribution (panel (e)), betweenness centrality (panel (f)), edge multiplicity distribution (panel (g)). We visualize the real-world (panel (d)) and deterministic (panel (h)) network, showing 0.25% of edges.

Anybeat was an online social network site. Nodes in the *anybeat* network [82] (Fig. 8) are users of this site. An edge between two nodes indicates that at least one of the nodes follows the other one. The DHG model (orange circles) is able to accurately capture the degree distribution (panel (a)), clustering (panel (c)), pairwise distance distribution (panel (e)), betweenness centrality (panel (f)), and edge multiplicity distribution (panel (g)) of the real-world network (blue squares). The network’s disassortativity is reproduced qualitatively (panel (b)) but shows quantitative disagreement. We also provide visualizations of the real-world (panel (d)) and deterministic (panel (h)) network, showing 0.35% of edges.

In the *bitcoin_trust* network [83] (Fig. 9) nodes are users of the Bitcoin OTC platform and edges encode trust between them. The DHG model (orange circles) can reproduce many features of the real-world network (blue squares), such as degree distribution (panel (a)), clustering (panel (c)), pairwise distance distribution (panel (e)), betweenness centrality (panel (f)). However, there

are discrepancies in the degree-degree correlations (panel (b)) and edge multiplicity distribution (panel (g)). We provide artistic visualizations of the real-world network (panel (d)) and its deterministic counterpart (panel (h)), showing 0.55% of edges.

b. Technological Networks

In the *linux* network [84] (Fig. 10) nodes are source files of the Linux operating system and there is an edge between two nodes if one of the source files includes the other. A graph from the DHG model (orange circles) with matched parameters reproduces many network properties of the real-world *linux* network (blue squares) including the degree distribution (panel (a)), average nearest neighbor degree (panel (b)), clustering (panel (c)), pairwise distances (panel (e)), betweenness centrality (panel (f)), and edge multiplicity distribution (panel (g)). We visualize the real-world network in panel (d) and the network from the DHG model in panel (h), showing 0.25% of edges.

In the *internet_as* network [85] (Fig. 11) is a map of the internet at the autonomous system level. Nodes are physical routers and two nodes are connected if they can directly exchange information with each other. We observe an excellent agreement between the real-world network (blue squares) and the one generated from the DHG model (orange circles) across many network prop-

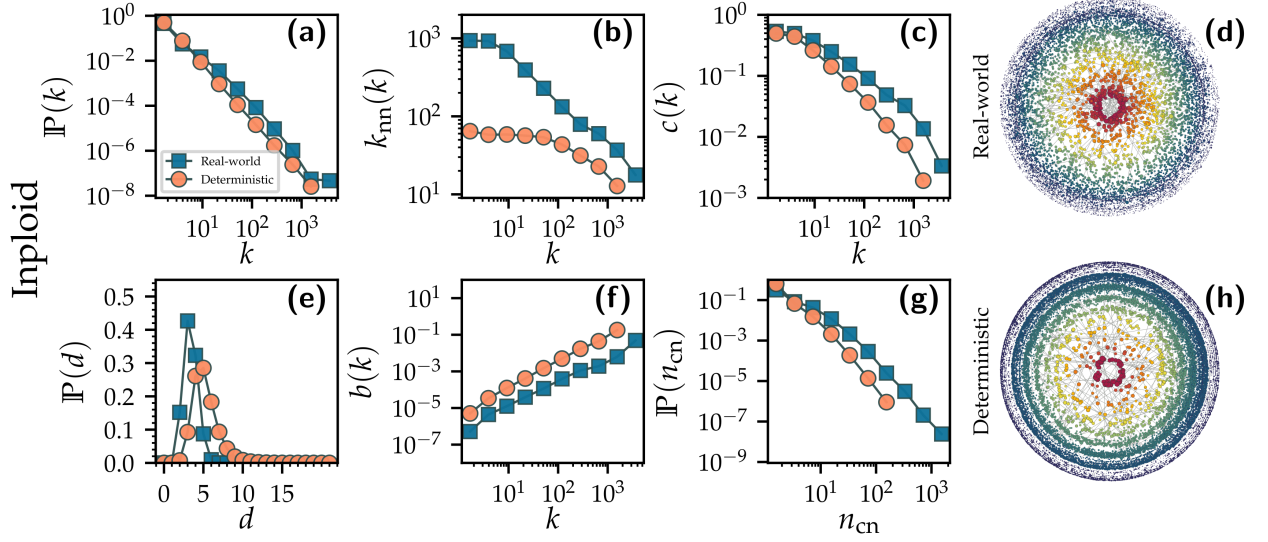


FIG. 6. Network properties (degree distribution $\mathbb{P}(k)$ (panel (a)), average nearest neighbor degree $k_{nn}(k)$ (panel (b)), local clustering $c(k)$ (panel (c)), pairwise distance distribution $\mathbb{P}(d)$ (panel (e)), betweenness centrality $b(k)$ (panel (f)), edge multiplicity distribution $\mathbb{P}(n_{cn})$ (panel (g))) of the **inploid** network [80] (blue squares) and a DHG graph (orange circles) with matching parameters, as well as artistic representations of the real-world (panel (d)) and deterministic (panel (h)) network.

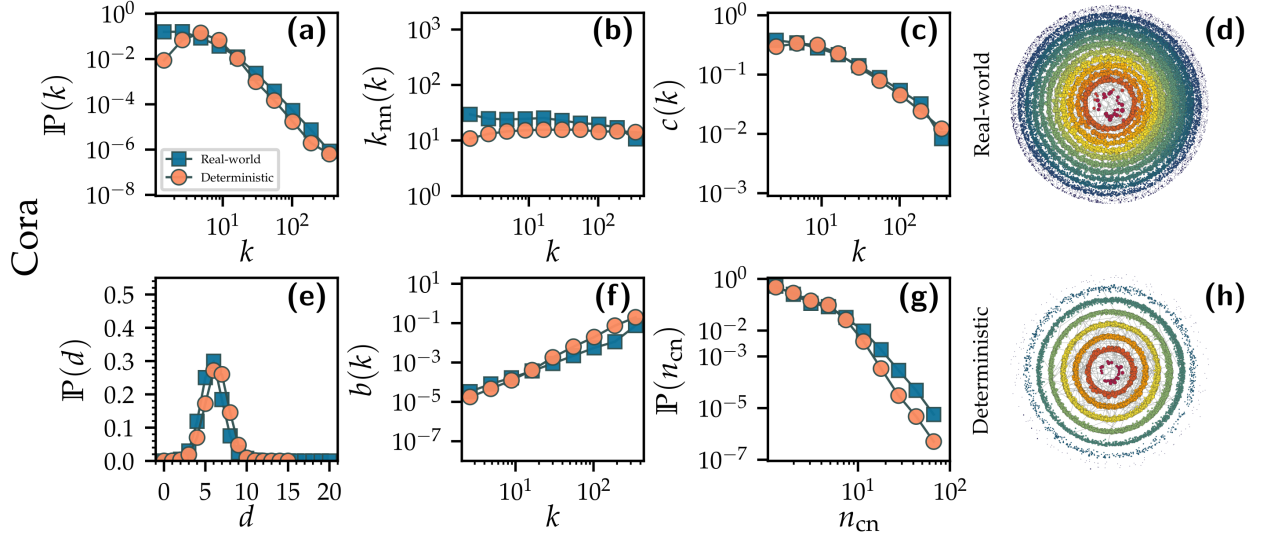


FIG. 7. Network properties (degree distribution $\mathbb{P}(k)$ (panel (a)), average nearest neighbor degree $k_{nn}(k)$ (panel (b)), local clustering $c(k)$ (panel (c)), pairwise distance distribution $\mathbb{P}(d)$ (panel (e)), betweenness centrality $b(k)$ (panel (f)), edge multiplicity distribution $\mathbb{P}(n_{cn})$ (panel (g))) of the **cora** network [81] (blue squares) and a DHG graph (orange circles) with matching parameters, as well as artistic representations of the real-world (panel (d)) and deterministic (panel (h)) network.

erties such as the degree distribution (panel (a)), average nearest neighbor degree (panel (b)), clustering (panel (c)), pairwise distances (panel (e)), betweenness centrality (panel (f)), and edge multiplicity distribution (panel (g)). We also provide visualizations of the real-world (panel (d)) and the deterministic network (panel (h)),

showing 0.35% of edges.

In the **google** network [86] (Fig. 12), nodes are google-internal webpages and edges represent hyperlinks between them. For this network dataset a wide range of network properties of the real-world network (blue squares) such as heterogeneous degree distribution (panel

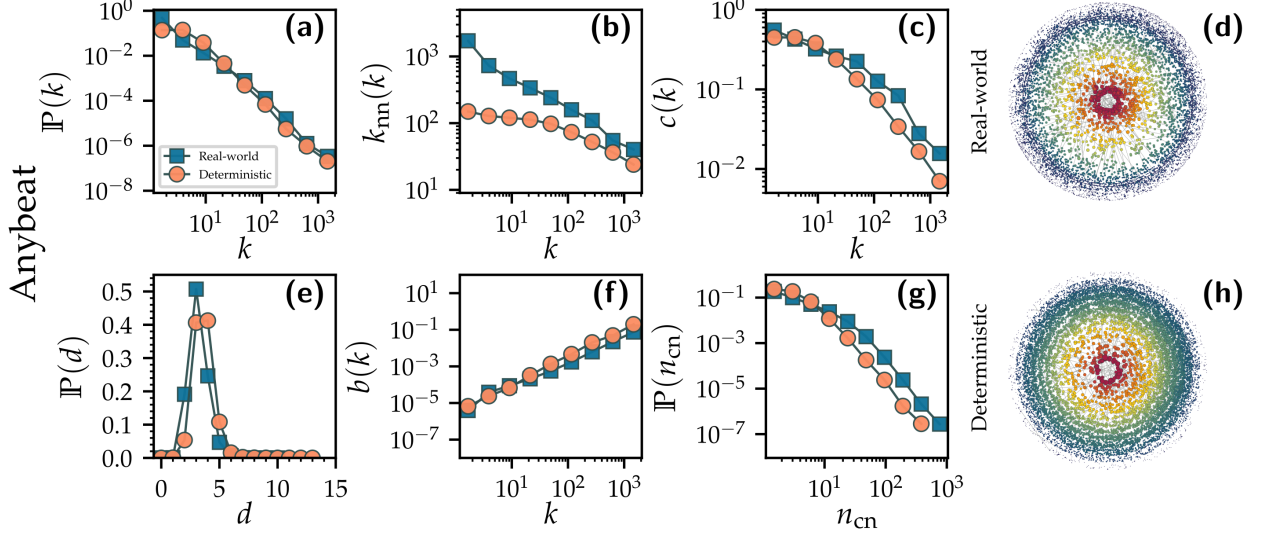


FIG. 8. Network properties (degree distribution $\mathbb{P}(k)$ (panel (a)), average nearest neighbor degree $k_{nn}(k)$ (panel (b)), local clustering $c(k)$ (panel (c)), pairwise distance distribution $\mathbb{P}(d)$ (panel (e)), betweenness centrality $b(k)$ (panel (f)), edge multiplicity distribution $\mathbb{P}(n_{cn})$ (panel (g))) of the **anybeat** network [82] (blue squares) and a DHG graph (orange circles) with matching parameters, as well as artistic representations of the real-world (panel (d)) and deterministic (panel (h)) network.

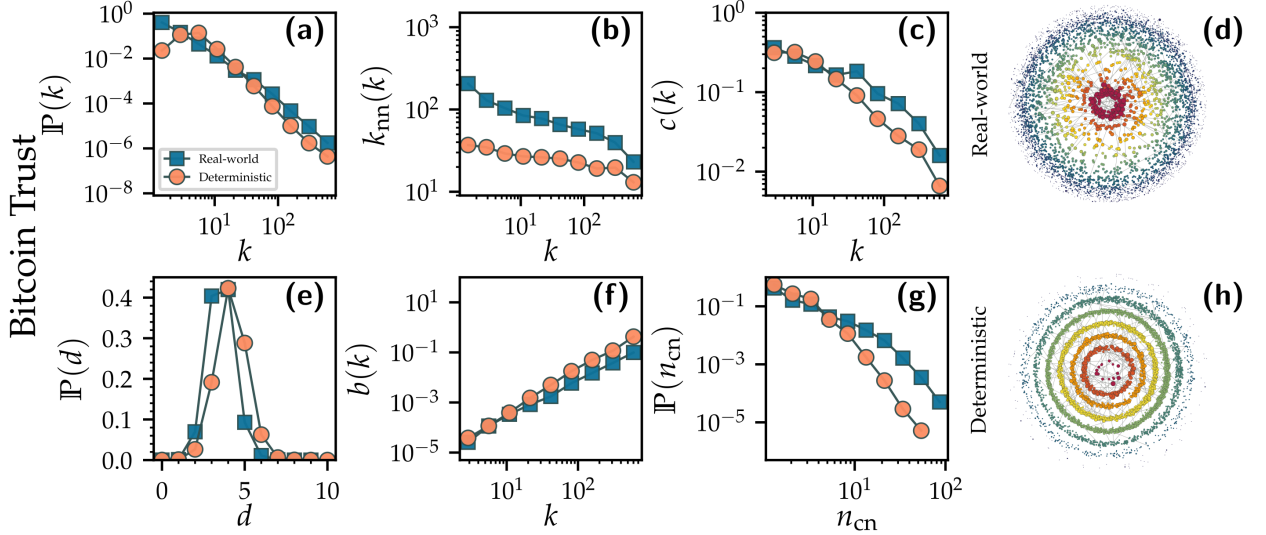


FIG. 9. Network properties (degree distribution $\mathbb{P}(k)$ (panel (a)), average nearest neighbor degree $k_{nn}(k)$ (panel (b)), local clustering $c(k)$ (panel (c)), pairwise distance distribution $\mathbb{P}(d)$ (panel (e)), betweenness centrality $b(k)$ (panel (f)), edge multiplicity distribution $\mathbb{P}(n_{cn})$ (panel (g))) of the **bitcoin_trust** network [83] (blue squares) and a DHG graph (orange circles) with matching parameters, as well as artistic representations of the real-world (panel (d)) and deterministic (panel (h)) network.

(a)), disassortativity (panel (b)), clustering (panel (c)), small-world behavior (panel (e)), betweenness (panel (f)), and edge multiplicity distribution (panel (g)) are well captured by the DHG model (orange circles). We also visualize the real-world (panel (d)) and determinis-

tic (panel (h)) network, showing 0.25% of edges.

The **jdk** network [84] (Fig. 13) represents software dependencies within the JDK framework. Each node in the network is a package and edges encode dependencies. The DHG model (orange circles) captures the real-world

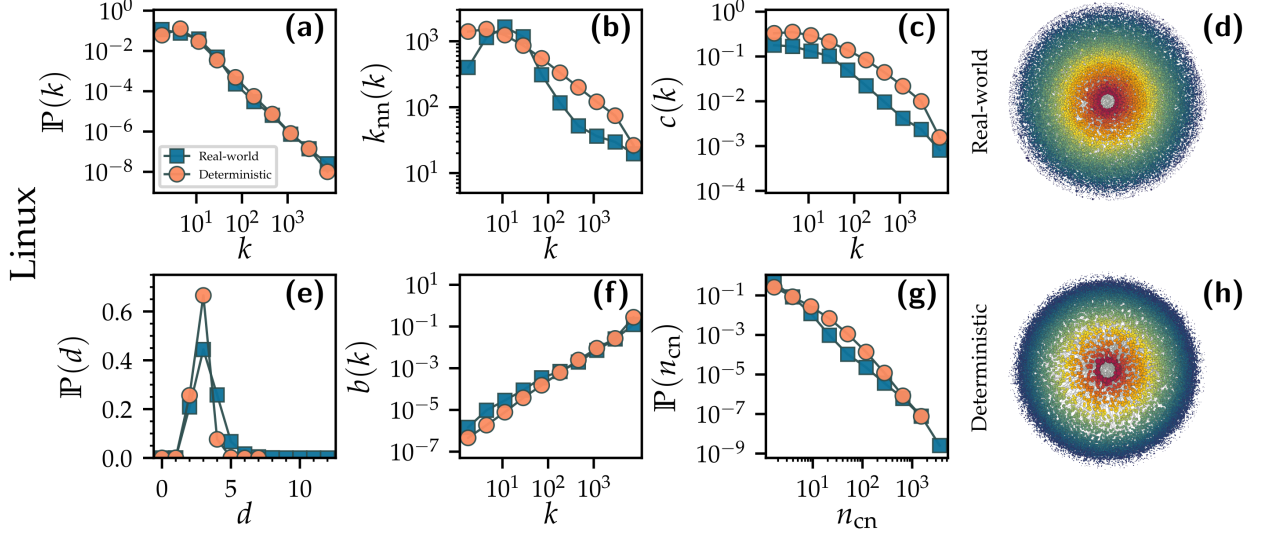


FIG. 10. Network properties (degree distribution $\mathbb{P}(k)$ (panel (a)), average nearest neighbor degree $k_{nn}(k)$ (panel (b)), local clustering $c(k)$ (panel (c)), pairwise distance distribution $\mathbb{P}(d)$ (panel (e)), betweenness centrality $b(k)$ (panel (f)), edge multiplicity distribution $\mathbb{P}(n_{cn})$ (panel (g))) of the **linux** network [84] (blue squares) and a DHG graph (orange circles) with matching parameters, as well as artistic representations of the real-world (panel (d)) and deterministic (panel (h)) network.

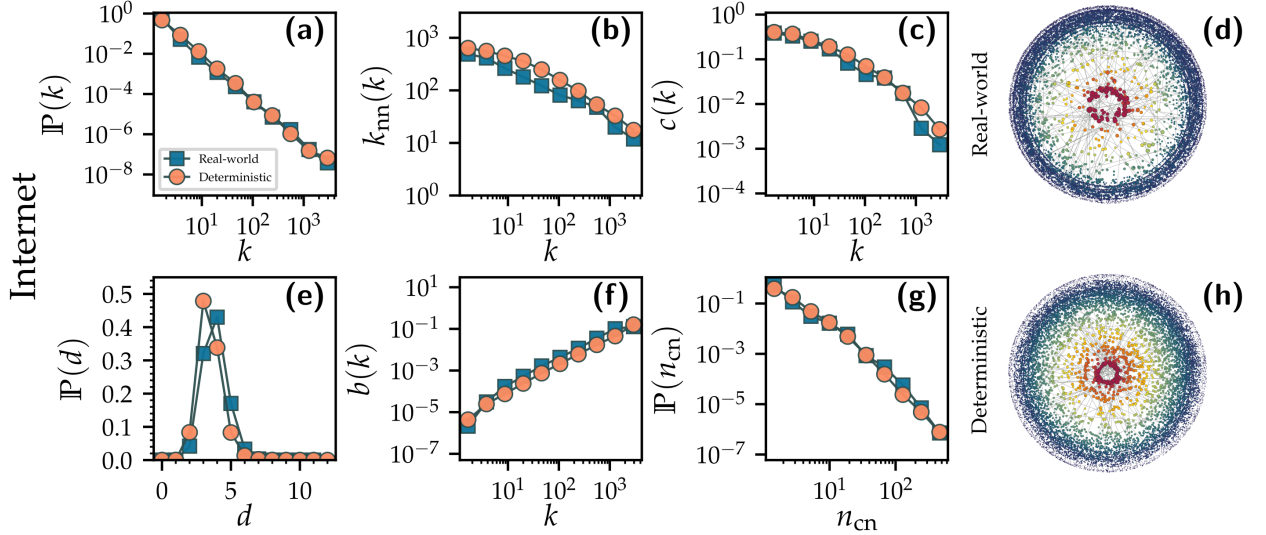


FIG. 11. Network properties (degree distribution $\mathbb{P}(k)$ (panel (a)), average nearest neighbor degree $k_{nn}(k)$ (panel (b)), local clustering $c(k)$ (panel (c)), pairwise distance distribution $\mathbb{P}(d)$ (panel (e)), betweenness centrality $b(k)$ (panel (f)), edge multiplicity distribution $\mathbb{P}(n_{cn})$ (panel (g))) of the **internet_as** network [85] (blue squares) and a DHG graph (orange circles) with matching parameters, as well as artistic representations of the real-world (panel (d)) and deterministic (panel (h)) network.

(blue squares) networks' broad degree distribution (panel (a)), disassortativity (panel (b)), clustering (panel (c)), small-world behavior (panel (e)), betweenness centrality (panel (f)), and to some extent also the edge multiplicity distribution (panel (g)). We provide visualization of the real-world network (panel (d)) and its deterministic

counterpart (panel (h)), showing 0.45% of edges.

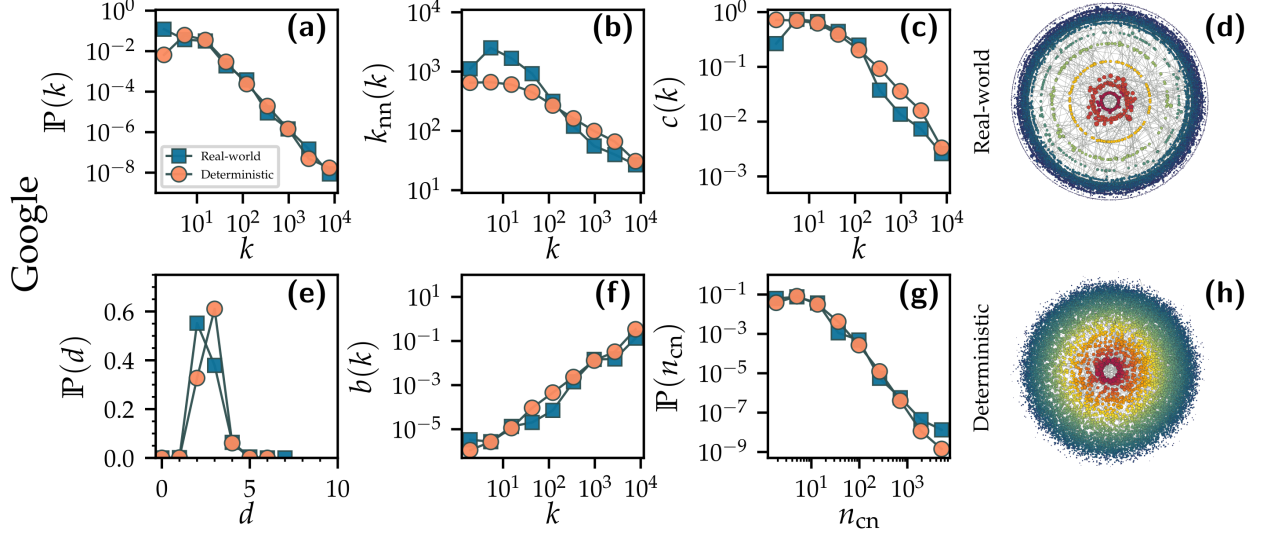


FIG. 12. Network properties (degree distribution $\mathbb{P}(k)$ (panel (a)), average nearest neighbor degree $k_{nn}(k)$ (panel (b)), local clustering $c(k)$ (panel (c)), pairwise distance distribution $\mathbb{P}(d)$ (panel (e)), betweenness centrality $b(k)$ (panel (f)), edge multiplicity distribution $\mathbb{P}(n_{cn})$ (panel (g))) of the **google** network [86] (blue squares) and a DHG graph (orange circles) with matching parameters, as well as artistic representations of the real-world (panel (d)) and deterministic (panel (h)) network.

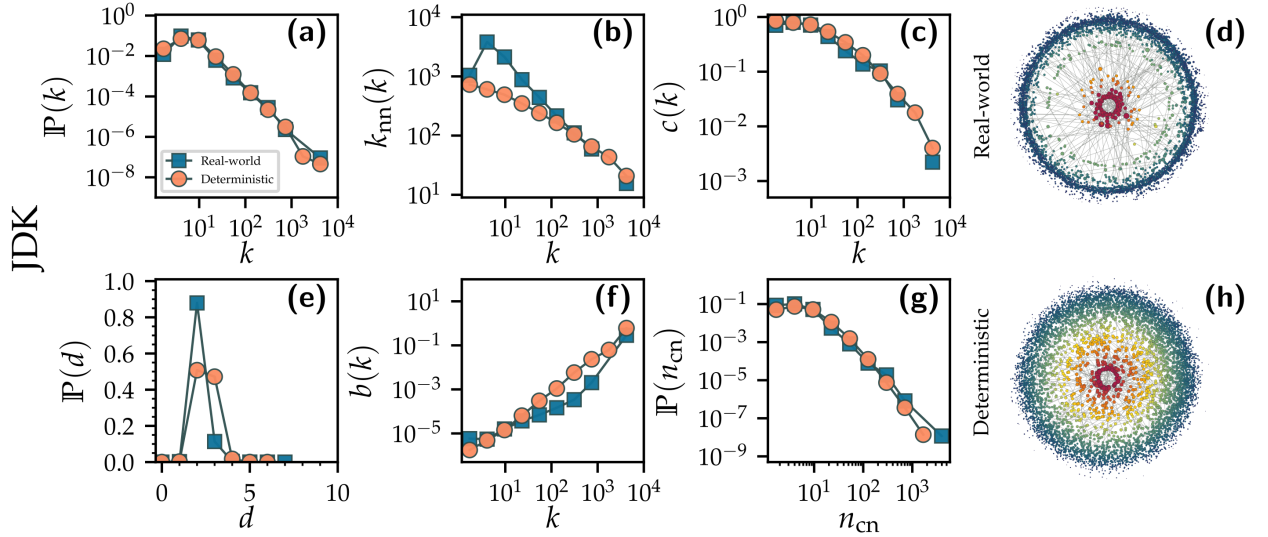


FIG. 13. Network properties (degree distribution $\mathbb{P}(k)$ (panel (a)), average nearest neighbor degree $k_{nn}(k)$ (panel (b)), local clustering $c(k)$ (panel (c)), pairwise distance distribution $\mathbb{P}(d)$ (panel (e)), betweenness centrality $b(k)$ (panel (f)), edge multiplicity distribution $\mathbb{P}(n_{cn})$ (panel (g))) of the **jdk** network [84] (blue squares) and a DHG graph (orange circles) with matching parameters, as well as artistic representations of the real-world (panel (d)) and deterministic (panel (h)) network.

c. Biological Networks

The **interactome.figeys** network [87] (Fig. 14) is a human protein-protein interaction network. Nodes represent proteins, and edges encode binding interactions between them. The DHG model (orange circles) repro-

duces the degree heterogeneity (panel (a)), distance distribution (panel (e)), and betweenness centrality (panel (f)) of the real-world network (blue squares) well. However, the dependence of average nearest neighbor degree (panel (b)) and clustering (panel (c)) on node degree are less well captured. The model also fails to capture

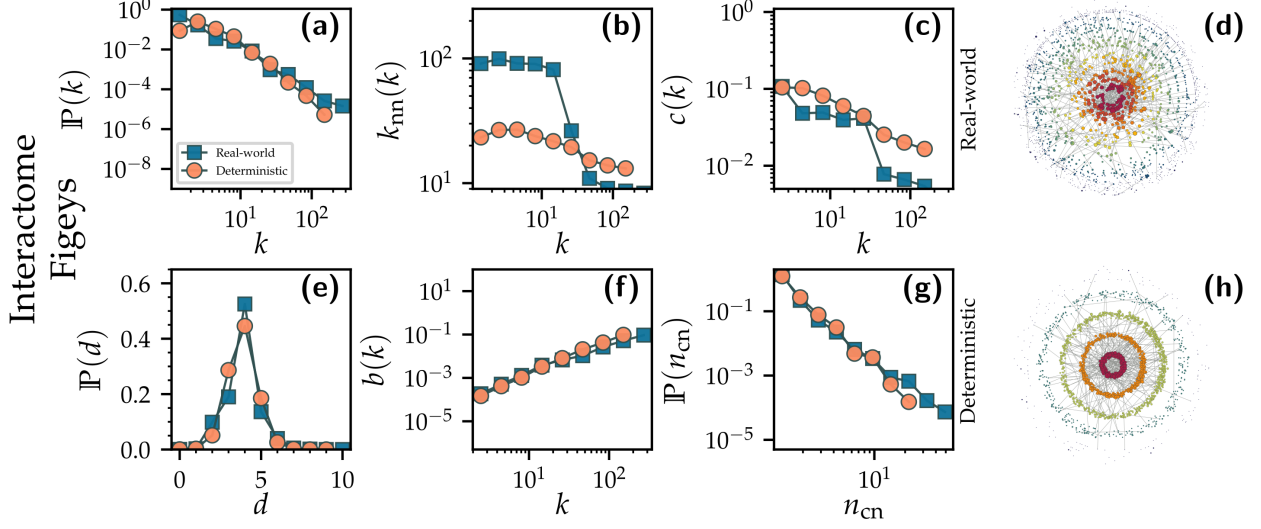


FIG. 14. Network properties (degree distribution $\mathbb{P}(k)$ (panel (a)), average nearest neighbor degree $k_{nn}(k)$ (panel (b)), local clustering $c(k)$ (panel (c)), pairwise distance distribution $\mathbb{P}(d)$ (panel (e)), betweenness centrality $b(k)$ (panel (f)), edge multiplicity distribution $\mathbb{P}(n_{cn})$ (panel (g))) of the `interactome_figey` network [87] (blue squares) and a DHG graph (orange circles) with matching parameters, as well as artistic representations of the real-world (panel (d)) and deterministic (panel (h)) network.

the tail of the edge multiplicity distribution (panel (g)). We visualize the real-world (panel (d)) and deterministic (panel (h)) network, showing 5% of edges.

The network `celegans_metabolic` [88] (Fig. 15) is the metabolic network of the *caenorhabditis elegans* (*C. elegans*). The DHG model (orange circles) reproduces many properties of the real-world network (blue squares). This includes the degree distribution (panel (a)), the dependence of average nearest neighbor degree (panel (b)) and clustering (panel (c)) on node degree, as well as the distance distribution (panel (e)), betweenness centrality (panel (f)), and edge multiplicity distribution (panel (g)). We provide visualizations of the real-world (panel (d)) and deterministic (panel (h)) network, showing 10% of edges.

The network `celegans_neural` [2, 89] (Fig. 16) is the neural network of the nematode *C. elegans*, an important model organism in biology. For this relatively small network ($n = 297$) the correspondence between the DHG model (orange circles) and the real-world network (blue squares) is less good: The shape of the degree distribution (panel (a)) differs especially at low degrees. The dependence of the average nearest neighbor degree (panel (b)) and clustering on degree (panel (c)) on node degree are poorly captured. However, the distance distribution (panel (e)), betweenness centrality (panel (f)), and edge multiplicity distribution (panel (g)) are nicely reproduced. We provide artistic visualizations of the real-world (panel (d)) and deterministic (panel (h)) networks, showing 10% of edges.

d. Literature & Words Networks

In the `marvel_universe` network [90] (Fig. 17), nodes are Marvel characters, and edges encode their co-appearance in the same comic book. The DHG model (orange circles) can capture some properties of the real-world network (blue squares) but not others: The degree distribution (panel (a)) and betweenness centrality (panel (f)) are reproduced well. The model also captures the degree-degree correlations (panel (b)) and pairwise distance distribution (panel (e)) to some extent. However, the real-world network seems to be tree-like. As a consequence we observe stark deviations in the clustering (panel (c)) and edge multiplicity distribution (panel (g)). We visualize both the real-world (panel (d)) and deterministic network (panel (h)), showing 0.45% of edges.

In the `bible_nouns` network [74] (Fig. 18), nodes are nouns, and edges encode their co-appearance in the same Bible verse. The real-world network (blue squares) is in many aspects well described by the DHG model (orange circles): This includes the degree distribution (panel (a)), absence of major degree correlations (panel (b)), clustering (panel (c)), small-worldness (panel (e)), betweenness (panel (f)), and edge multiplicity distribution (panel (g)). We visualize the real-world (panel (d)) and deterministic (panel (h)) network, showing 2% of edges.

In the `game_thrones` network [91] (Fig. 19), nodes are characters in the novel *A Storm of Swords* from the Game of Thrones franchise, and edges encode that both characters are mentioned within 15 words of each other. Given

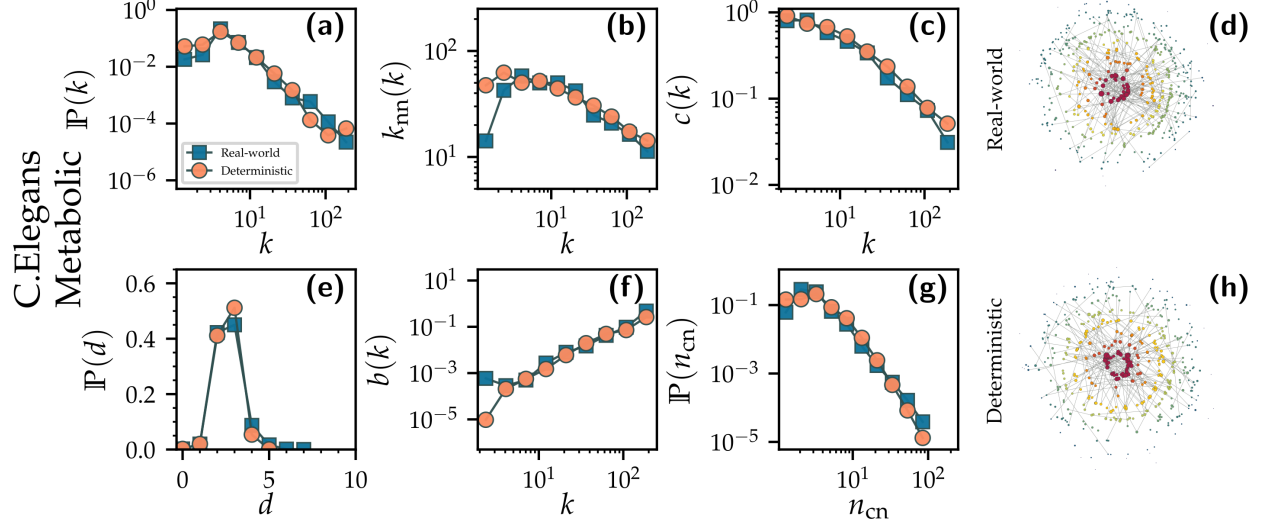


FIG. 15. Network properties (degree distribution $\mathbb{P}(k)$ (panel (a)), average nearest neighbor degree $k_{nn}(k)$ (panel (b)), local clustering $c(k)$ (panel (c)), pairwise distance distribution $\mathbb{P}(d)$ (panel (e)), betweenness centrality $b(k)$ (panel (f)), edge multiplicity distribution $\mathbb{P}(n_{cn})$ (panel (g))) of the *celegans_metabolic* network [88] (blue squares) and a DHG graph (orange circles) with matching parameters, as well as artistic representations of the real-world (panel (d)) and deterministic (panel (h)) network.

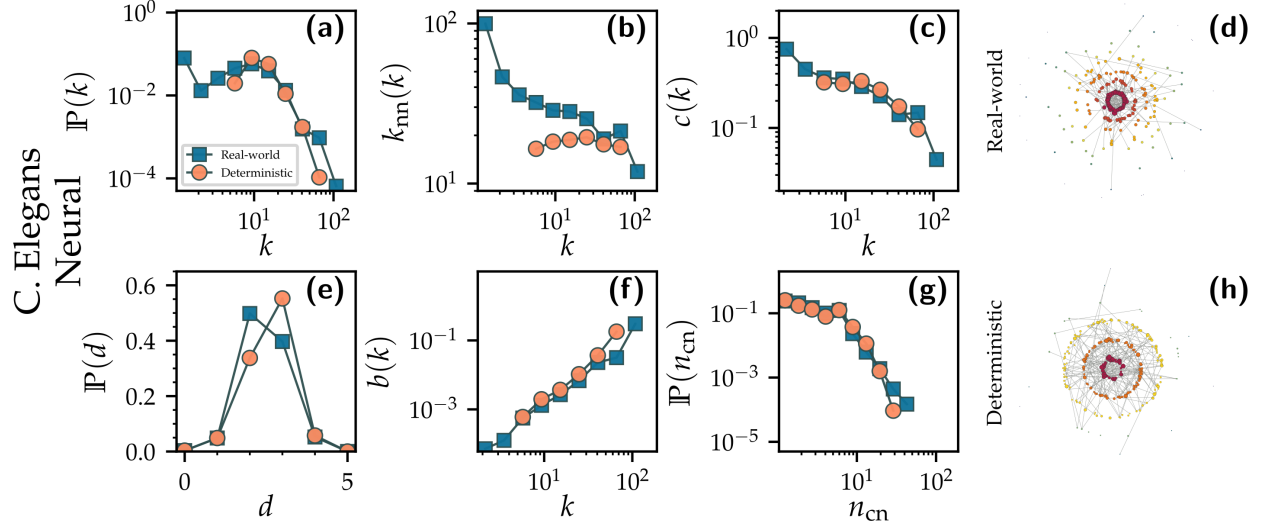


FIG. 16. Network properties (degree distribution $\mathbb{P}(k)$ (panel (a)), average nearest neighbor degree $k_{nn}(k)$ (panel (b)), local clustering $c(k)$ (panel (c)), pairwise distance distribution $\mathbb{P}(d)$ (panel (e)), betweenness centrality $b(k)$ (panel (f)), edge multiplicity distribution $\mathbb{P}(n_{cn})$ (panel (g))) of the *celegans_neural* network [2, 89] (blue squares) and a DHG graph (orange circles) with matching parameters, as well as artistic representations of the real-world (panel (d)) and deterministic (panel (h)) network.

the small size of this network ($n = 107$), we observe a very good correspondence between the real-world (blue squares) and deterministic (orange circles) networks in terms of their network properties including degree distribution (panel (a)), absence of degree-degree correlations

(panel (b)), clustering (panel (c)), pairwise distance distribution (panel (e)), betweenness centrality (panel (f)), and edge multiplicity distribution (panel (g)). We visualize both the real-world (panel (d)) and deterministic (panel (h)) networks, showing 50% of edges.

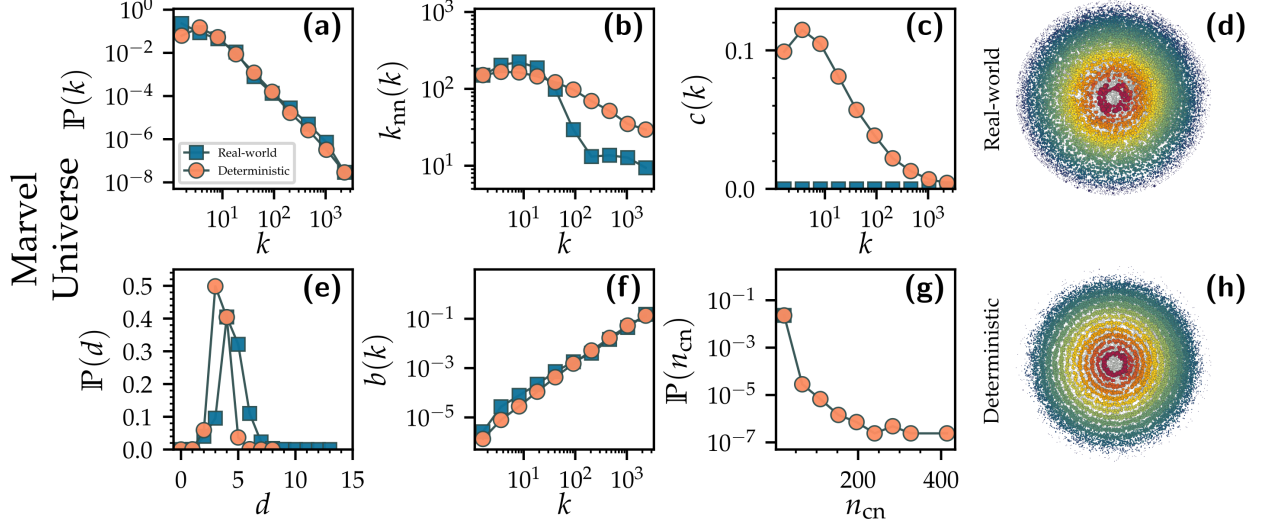


FIG. 17. Network properties (degree distribution $\mathbb{P}(k)$ (panel (a)), average nearest neighbor degree $k_{nn}(k)$ (panel (b)), local clustering $c(k)$ (panel (c)), pairwise distance distribution $\mathbb{P}(d)$ (panel (e)), betweenness centrality $b(k)$ (panel (f)), edge multiplicity distribution $\mathbb{P}(n_{cn})$ (panel (g))) of the `marvel_universe` network [90] (blue squares) and a DHG graph (orange circles) with matching parameters, as well as artistic representations of the real-world (panel (d)) and deterministic (panel (h)) network.

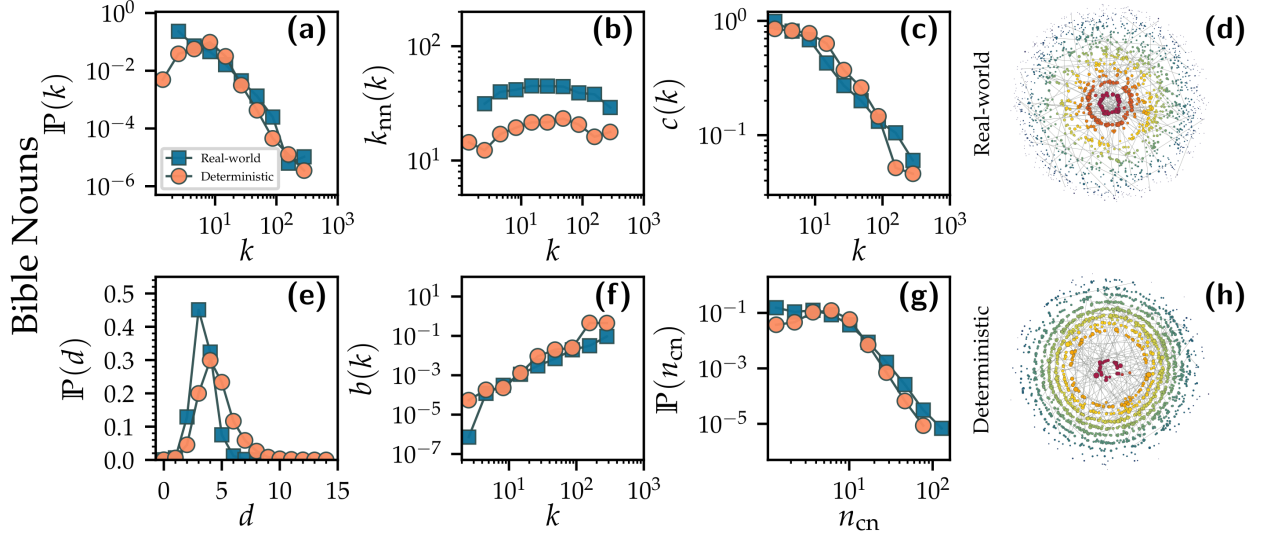


FIG. 18. Network properties (degree distribution $\mathbb{P}(k)$ (panel (a)), average nearest neighbor degree $k_{nn}(k)$ (panel (b)), local clustering $c(k)$ (panel (c)), pairwise distance distribution $\mathbb{P}(d)$ (panel (e)), betweenness centrality $b(k)$ (panel (f)), edge multiplicity distribution $\mathbb{P}(n_{cn})$ (panel (g))) of the `bible_nouns` network [74] (blue squares) and a DHG graph (orange circles) with matching parameters, as well as artistic representations of the real-world (panel (d)) and deterministic (panel (h)) network.

e. Transportation Networks

In the `faa_routes` [74] dataset (Fig. 20), nodes are airports, and edges encode the preferred routes between them. The degree distribution (panel (a)) of the real-

world network (blue squares) lacks heavy tails and is less well described by the DHG model (orange circles). Similarly, the degree-correlations (panel (b)), clustering (panel (c)), and betweenness centrality (panel (f)) are only roughly reproduced. The models edge multiplic-

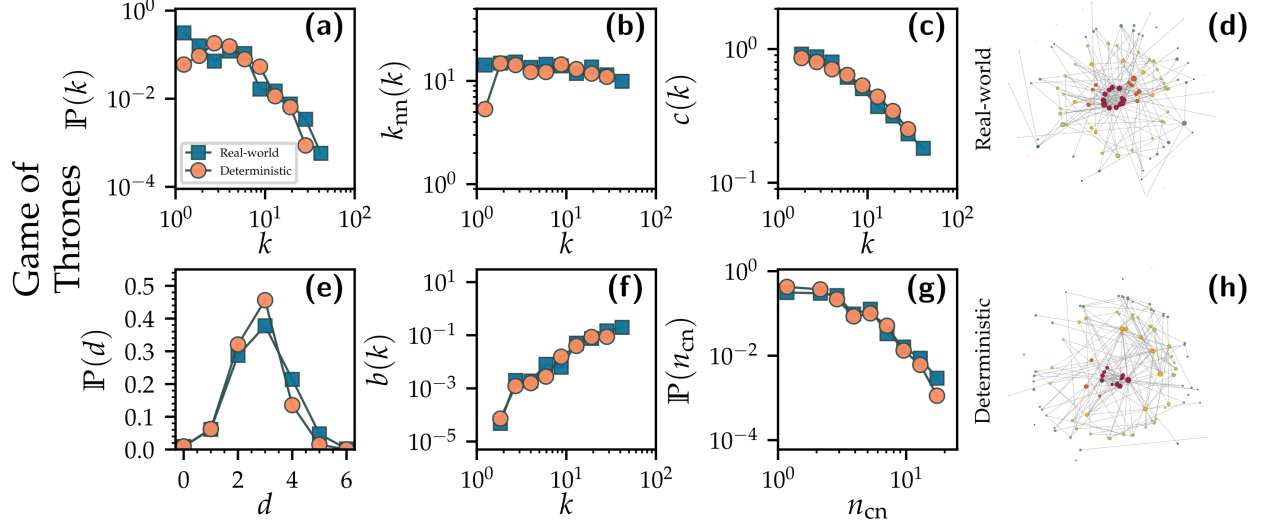


FIG. 19. Network properties (degree distribution $\mathbb{P}(k)$ (panel (a)), average nearest neighbor degree $k_{nn}(k)$ (panel (b)), local clustering $c(k)$ (panel (c)), pairwise distance distribution $\mathbb{P}(d)$ (panel (e)), betweenness centrality $b(k)$ (panel (f)), edge multiplicity distribution $\mathbb{P}(n_{cn})$ (panel (g))) of the **game_thrones** network [91] (blue squares) and a DHG graph (orange circles) with matching parameters, as well as artistic representations of the real-world (panel (d)) and deterministic (panel (h)) network.

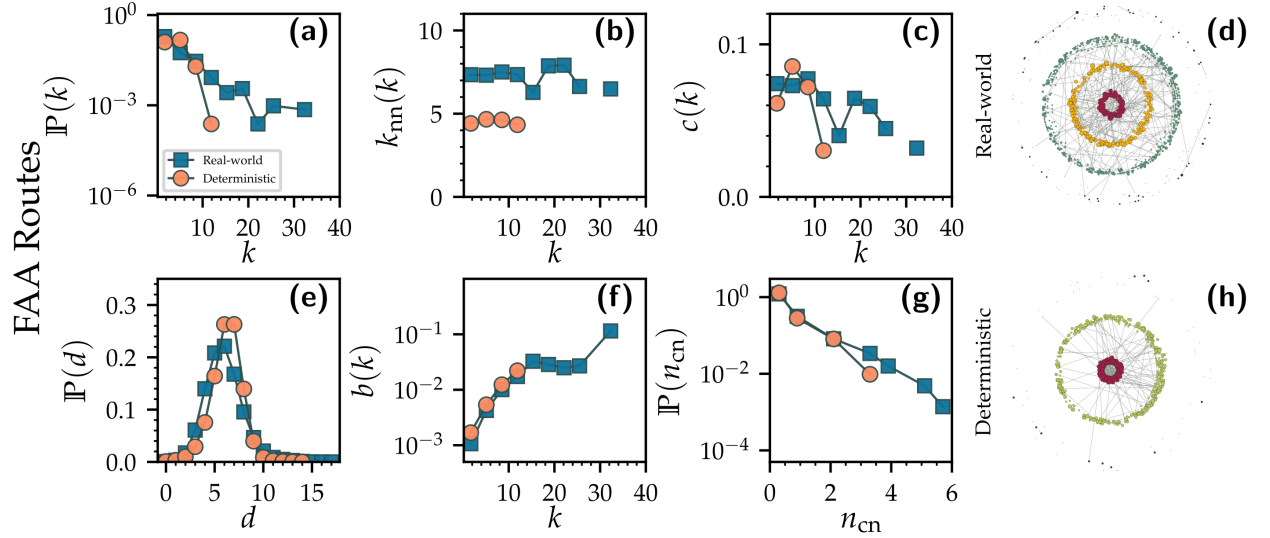


FIG. 20. Network properties (degree distribution $\mathbb{P}(k)$ (panel (a)), average nearest neighbor degree $k_{nn}(k)$ (panel (b)), local clustering $c(k)$ (panel (c)), pairwise distance distribution $\mathbb{P}(d)$ (panel (e)), betweenness centrality $b(k)$ (panel (f)), edge multiplicity distribution $\mathbb{P}(n_{cn})$ (panel (g))) of the **faa_routes** network [74] (blue squares) and a DHG graph (orange circles) with matching parameters, as well as artistic representations of the real-world (panel (d)) and deterministic (panel (h)) network.

ity distribution (panel (g)) is slightly less heterogeneous. However, the pairwise distance distribution (panel (e)) is accurately captured by the model. We also show artistic visualizations of the real-world (panel (d)) and deterministic (panel (h)) network, showing 10% of edges.

In the **euroroads** network [92] (Fig. 21), nodes are

cities, and edges encode international E-roads between them. The DHG model (orange circles) can reproduce some aspects of the real-world network (blue squares), e.g., the degree distribution (panel (a)), absence of degree correlations (panel (b)), and the edge multiplicity distribution (panel (g)). The model does not capture

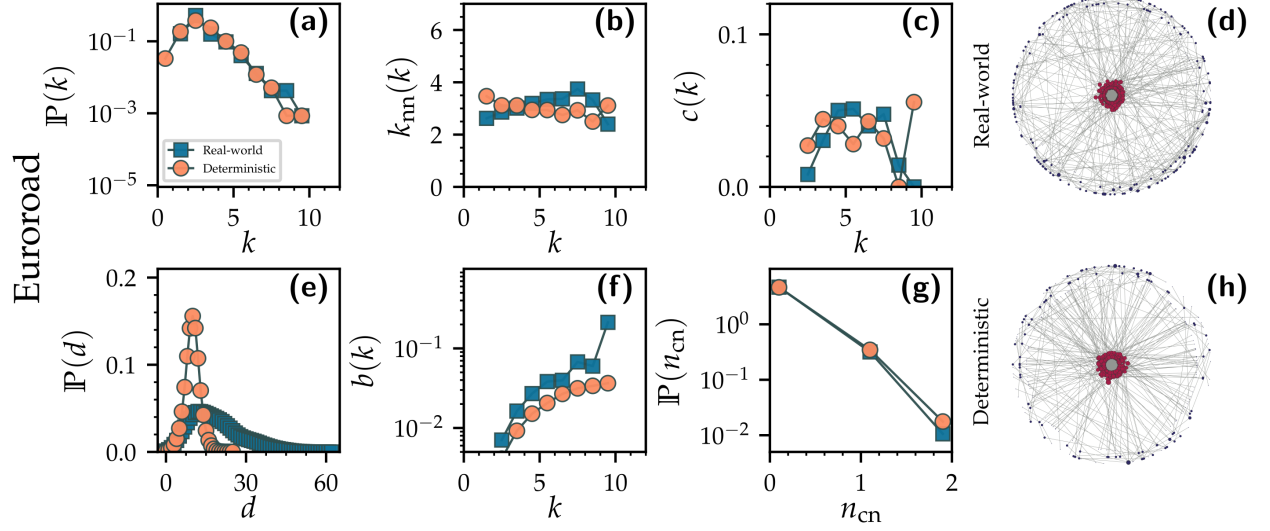


FIG. 21. Network properties (degree distribution $\mathbb{P}(k)$ (panel (a)), average nearest neighbor degree $k_{nn}(k)$ (panel (b)), local clustering $c(k)$ (panel (c)), pairwise distance distribution $\mathbb{P}(d)$ (panel (e)), betweenness centrality $b(k)$ (panel (f)), edge multiplicity distribution $\mathbb{P}(n_{cn})$ (panel (g))) of the **euroroad** network [92] (blue squares) and a DHG graph (orange circles) with matching parameters, as well as artistic representations of the real-world (panel (d)) and deterministic (panel (h)) network.

the clustering (panel (c)) and the betweenness centrality (panel (f)) well. Also the distance distribution is very different (panel (e)). This is expected as the underlying metric space that governs connections in the road network is Euclidean not hyperbolic. We visualize the real-world (panel (d)) and deterministic (panel (h)) network, showing all edges.

In the **london_transport** network [93] (Fig. 22), nodes are public transportation stations in London, and edges encode connections between them via one of three means of transportation. The DHG model (orange circles) appears to be a poor model of the real-world network (blue squares): While it can capture qualitative features of the degree distribution (panel (a)), average nearest neighbor degree (panel (b)), clustering (panel (c)), betweenness centrality (panel (f)), and edge multiplicity distribution (panel (g)), there are substantial quantitative difference. Moreover, the pairwise distance distribution (panel (e)) of the real-world network differs from the one under the model. We provide visualizations of the real-world (panel (d)) and deterministic (panel (h)) network, showing 50% of edges.

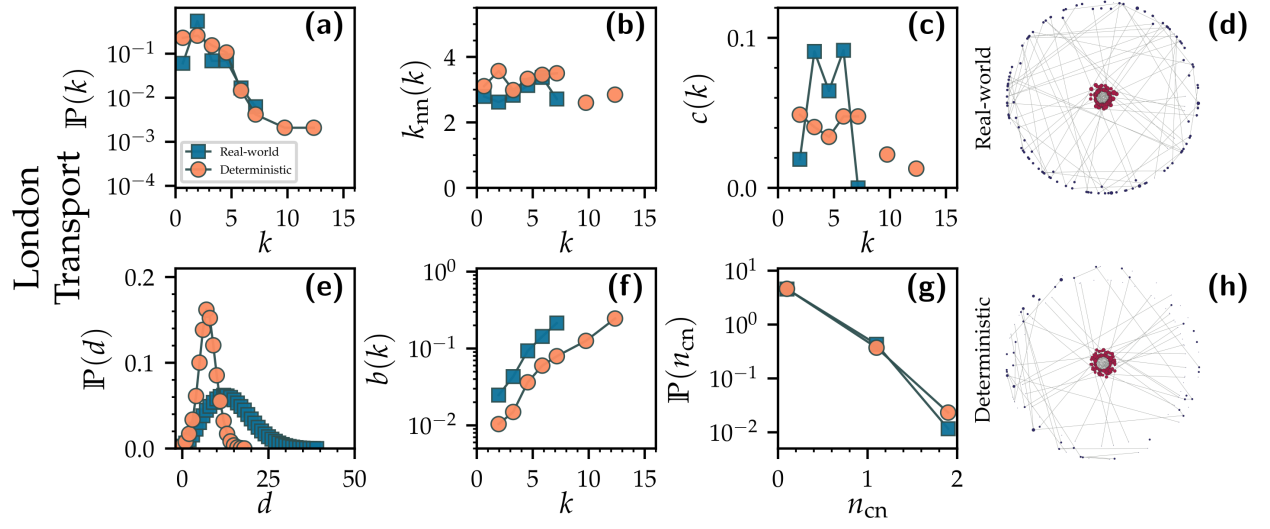


FIG. 22. Network properties (degree distribution $\mathbb{P}(k)$ (panel (a)), average nearest neighbor degree $k_{nn}(k)$ (panel (b)), local clustering $c(k)$ (panel (c)), pairwise distance distribution $\mathbb{P}(d)$ (panel (e)), betweenness centrality $b(k)$ (panel (f)), edge multiplicity distribution $\mathbb{P}(n_{cn})$ (panel (g))) of the `london_transport` network [93] (blue squares) and a DHG graph (orange circles) with matching parameters, as well as artistic representations of the real-world (panel (d)) and deterministic (panel (h)) network.

- [1] G. Cimini, T. Squartini, F. Saracco, D. Garlaschelli, A. Gabrielli, and G. Caldarelli, The statistical physics of real-world networks, *Nature Reviews Physics* **1**, 58 (2019).
- [2] D. J. Watts and S. H. Strogatz, Collective dynamics of ‘small-world’ networks, *Nature* **393**, 440 (1998).
- [3] A.-L. Barabási and R. Albert, Emergence of Scaling in Random Networks, *Science* **286**, 509 (1999).
- [4] T. Watanabe, S. Hirose, H. Wada, Y. Imai, T. Machida, I. Shirouzu, S. Konishi, Y. Miyashita, and N. Masuda, A pairwise maximum entropy model accurately describes resting-state human brain networks, *Nature Communications* **4**, 1370 (2013).
- [5] K. Anand and G. Bianconi, Gibbs entropy of network ensembles by cavity methods, *Physical Review E* **82**, 011116 (2010).
- [6] T. Squartini and D. Garlaschelli, Analytical maximum-likelihood method to detect patterns in real networks, *New Journal of Physics* **13**, 083001 (2011).
- [7] G. Cimini, A. Carra, L. Didomenicantonio, and A. Zaccaria, Meta-validation of bipartite network projections, *Communications Physics* **5**, 76 (2022).
- [8] P. Villegas, T. Gili, G. Caldarelli, and A. Gabrielli, Laplacian renormalization group for heterogeneous networks, *Nature Physics* **19**, 445 (2023).
- [9] S. Popescu, A. J. Short, and A. Winter, Entanglement and the foundations of statistical mechanics, *Nature Physics* **2**, 754 (2006).
- [10] S. Goldstein, J. L. Lebowitz, R. Tumulka, and N. Zanghi, Canonical Typicality, *Physical Review Letters* **96**, 050403 (2006).
- [11] P. Reimann, Typicality for Generalized Microcanonical Ensembles, *Physical Review Letters* **99**, 160404 (2007).
- [12] M. Rigol, V. Dunjko, and M. Olshanii, Thermalization and its mechanism for generic isolated quantum systems, *Nature* **452**, 854 (2008).
- [13] P. Boes, H. Wilming, J. Eisert, and R. Gallego, Statistical ensembles without typicality, *Nature Communications* **9**, 1022 (2018).
- [14] M. Schröder, S. H. E. Rahbari, and J. Nagler, Crackling noise in fractional percolation, *Nature Communications* **4**, 2222 (2013).
- [15] P. Henderson, R. Islam, P. Bachman, J. Pineau, D. Precup, and D. Meger, Deep reinforcement learning that matters, in *Proceedings of the AAAI Conference on Artificial Intelligence*, Vol. 32 (2018).
- [16] Moving towards reproducible machine learning, *Nature Computational Science* **1**, 629 (2021).
- [17] G. Piantadosi, S. Marrone, and C. Sansone, On Reproducibility of Deep Convolutional Neural Networks Approaches, in *Reproducible Research in Pattern Recognition*, Vol. 11455, edited by B. Kerautret, M. Colom, D. Lopresti, P. Monasse, and H. Talbot (Springer International Publishing, Cham, 2019) pp. 104–109.
- [18] S. Hoory, N. Linial, and A. Wigderson, Expander graphs and their applications, *Bulletin of the American Mathematical Society* **43**, 439 (2006).
- [19] A. Thomason, Pseudo-Random Graphs, in *North-Holland Mathematics Studies*, Vol. 144 (Elsevier, 1987) pp. 307–331.
- [20] F. R. K. Chung, R. L. Graham, and R. M. Wilson, Quasi-random graphs, *Proceedings of the National Academy of Sciences* **85**, 969 (1988).
- [21] M. Krivelevich and B. Sudakov, Pseudo-random Graphs, in *More Sets, Graphs and Numbers: A Salute to Vera Sós and András Hajnal*, edited by E. Györi, G. O. H. Katona, L. Lovász, and T. Fleiner (Springer, Berlin, Heidelberg, 2006) pp. 199–262.
- [22] J. Park and M. E. J. Newman, Statistical mechanics of networks, *Physical Review E* **70**, 066117 (2004).
- [23] G. Bianconi, Entropy of network ensembles, *Physical Review E* **79**, 036114 (2009).
- [24] P. L. Krapivsky and S. Redner, Organization of growing random networks, *Physical Review E* **63**, 066123 (2001).
- [25] C. Orsini, M. M. Dankulov, P. Colomer-de-Simón, A. Jmakovic, P. Mahadevan, A. Vahdat, K. E. Bassler, Z. Toroczkai, M. Boguñá, G. Caldarelli, S. Fortunato, and D. Krioukov, Quantifying randomness in real networks, *Nature Communications* **6**, 8627 (2015).
- [26] P. Erdős and A. Rényi, On the evolution of random graphs, *Publications of the Mathematical Institute of the Hungarian Academy of Sciences* **5**, 17 (1960).
- [27] T. M. Cover and J. A. Thomas, *Elements of Information Theory*, 1st ed. (Wiley, 2005).
- [28] D. J. C. MacKay, *Information Theory, Inference and Learning Algorithms* (Cambridge University Press, Cambridge, UK, 2003).
- [29] E. T. Jaynes, Information Theory and Statistical Mechanics, *Physical Review* **106**, 620 (1957).
- [30] M. Kardar, *Statistical Physics of Particles*, 1st ed. (Cambridge University Press, 2007).
- [31] M. R. Garey and D. S. Johnson, *Computers and Intractability; A Guide to the Theory of NP-Completeness* (W. H. Freeman & Co., USA, 1990).
- [32] H. M. Salkin and C. A. De Kluyver, The knapsack problem: A survey, *Naval Research Logistics Quarterly* **22**, 127 (1975).
- [33] L. Devroye, *Non-Uniform Random Variate Generation* (Springer New York, New York, NY, 1986).
- [34] D. E. Knuth, *The art of computer programming, volume 2 (3rd ed.): seminumerical algorithms* (Addison-Wesley Longman Publishing Co., Inc., USA, 1997).
- [35] G. Caldarelli, A. Capocci, P. De Los Rios, and M. A. Muñoz, Scale-Free Networks from Varying Vertex Intrinsic Fitness, *Physical Review Letters* **89**, 258702 (2002).
- [36] B. Söderberg, General formalism for inhomogeneous random graphs, *Physical Review E* **66**, 066121 (2002).
- [37] M. Boguñá and R. Pastor-Satorras, Class of correlated random networks with hidden variables, *Physical Review E* **68**, 036112 (2003).
- [38] M. Evans and J. S. Rosenthal, *Probability and Statistics: The Science of Uncertainty*, 2nd ed. (W.H. Freeman and Co., New York, 2010).
- [39] G. Last and M. Penrose, *Lectures on the Poisson Process*, Institute of Mathematical Statistics Textbooks (Cambridge University Press, Cambridge, 2017).
- [40] D. Krioukov, F. Papadopoulos, M. Kitsak, A. Vahdat, and M. Boguñá, Hyperbolic geometry of complex networks, *Physical Review E* **82**, 036106 (2010).
- [41] M. Boguñá, I. Bonamassa, M. De Domenico, S. Havlin, D. Krioukov, and M. Á. Serrano, Network geometry, *Nature Reviews Physics* **3**, 114 (2021).

- [42] G. Budel, M. Kitsak, R. Aldecoa, K. Zuev, and D. Krioukov, Random hyperbolic graphs in $d + 1$ dimensions, *Physical Review E* **109**, 054131 (2024).
- [43] M. Laber, *Deterministic Hyperbolic Graph Generator* (2025).
- [44] V. Zlatić, D. Garlaschelli, and G. Caldarelli, Networks with arbitrary edge multiplicities, *Europhysics Letters* **97**, 28005 (2012).
- [45] H. Hartle, B. Klein, S. McCabe, A. Daniels, G. St-Onge, C. Murphy, and L. Hébert-Dufresne, Network comparison and the within-ensemble graph distance, *Proceedings of the Royal Society A: Mathematical, Physical and Engineering Sciences* **476**, 20190744 (2020).
- [46] S. McCabe, L. Torres, T. LaRock, S. Haque, C.-H. Yang, H. Hartle, and B. Klein, Netrd: A library for network reconstruction and graph distances, *Journal of Open Source Software* **6**, 2990 (2021).
- [47] P. D. Grünwald, *The Minimum Description Length Principle* (The MIT Press, 2007).
- [48] P. Gacs, J. Tromp, and P. Vitanyi, Algorithmic statistics, *IEEE Transactions on Information Theory* **47**, 2443 (2001).
- [49] S. F. Edwards and P. W. Anderson, Theory of spin glasses, *Journal of Physics F: Metal Physics* **5**, 965 (1975).
- [50] S. P. Vadhan, Pseudorandomness, *Foundations and Trends in Theoretical Computer Science* **7**, 1 (2012).
- [51] E. T. Jaynes, *Probability Theory: The Logic of Science*, 1st ed., edited by G. L. Bretthorst (Cambridge University Press, 2003).
- [52] P. W. Holland and S. Leinhardt, An Exponential Family of Probability Distributions for Directed Graphs, *Journal of the American Statistical Association* **76**, 33 (1981).
- [53] O. Frank and D. Strauss, Markov Graphs, *Journal of the American Statistical Association* **81**, 832 (1986).
- [54] L. Meshulam and W. Bialek, Statistical mechanics for networks of real neurons, *Reviews of Modern Physics* **97**, 045002 (2025).
- [55] G. Robins, P. Pattison, Y. Kalish, and D. Lusher, An introduction to exponential random graph (p^*) models for social networks, *Social Networks Special Section: Advances in Exponential Random Graph (P^*) Models*, **29**, 173 (2007).
- [56] D. Lusher, J. Koskinen, and G. Robins, eds., *Exponential Random Graph Models for Social Networks: Theory, Methods, and Applications*, 1st ed. (Cambridge University Press, 2012).
- [57] T. Squartini and D. Garlaschelli, *Maximum-Entropy Networks: Pattern Detection, Network Reconstruction and Graph Combinatorics*, SpringerBriefs in Complexity (Springer International Publishing, Cham, 2017).
- [58] D. Garlaschelli and M. I. Loffredo, Generalized Bose-Fermi Statistics and Structural Correlations in Weighted Networks, *Physical Review Letters* **102**, 038701 (2009).
- [59] D. Garlaschelli and M. I. Loffredo, Multispecies grand-canonical models for networks with reciprocity, *Physical Review E* **73**, 015101 (2006).
- [60] C. P. Robert and G. Casella, *Monte Carlo Statistical Methods*, Springer Texts in Statistics (Springer New York, New York, NY, 1999).
- [61] E. N. Gilbert, Random Graphs, *The Annals of Mathematical Statistics* **30**, 1141 (1959).
- [62] P. van der Hoorn, G. Lippner, and D. Krioukov, Sparse Maximum-Entropy Random Graphs with a Given Power-Law Degree Distribution, *Journal of Statistical Physics* **173**, 806 (2018).
- [63] B. Karrer and M. E. J. Newman, Stochastic blockmodels and community structure in networks, *Physical Review E* **83**, 016107 (2011).
- [64] M. Penrose, *Random Geometric Graphs* (Oxford University Press, 2003).
- [65] M. D. Penrose, Connectivity of soft random geometric graphs, *The Annals of Applied Probability* **26**, 986 (2016).
- [66] M. Á. Serrano, D. Krioukov, and M. Boguñá, Self-Similarity of Complex Networks and Hidden Metric Spaces, *Physical Review Letters* **100**, 078701 (2008).
- [67] H. A. David and H. N. Nagaraja, *Order Statistics*, 1st ed., Wiley Series in Probability and Statistics (Wiley, 2003).
- [68] A. M. Mathai, *An Introduction to Geometrical Probability: Distributional Aspects with Applications*, Statistical Distributions and Models with Applications No. 1 (Gordon and Breach, Amsterdam, 1999).
- [69] M. Á. Serrano and M. Boguñá, *The Shortest Path to Network Geometry: A Practical Guide to Basic Models and Applications*, 1st ed. (Cambridge University Press, 2022).
- [70] I. Voitalov, P. van der Hoorn, R. van der Hofstad, and D. Krioukov, Scale-free networks well done, *Physical Review Research* **1**, 033034 (2019).
- [71] I. Voitalov, Tail-estimation, <https://github.com/ivanvoitalov/tail-estimation> (2025).
- [72] R. P. Brent, *Algorithms for Minimization Without Derivatives* (Courier Corporation, 2013).
- [73] P. Virtanen, R. Gommers, T. E. Oliphant, M. Haberland, T. Reddy, D. Cournapeau, E. Burovski, P. Peterson, W. Weckesser, J. Bright, S. J. van der Walt, M. Brett, J. Wilson, K. J. Millman, N. Mayorov, A. R. J. Nelson, E. Jones, R. Kern, E. Larson, C. J. Carey, Í. Polat, Y. Feng, E. W. Moore, J. VanderPlas, D. Laxalde, J. Perktold, R. Cimrman, I. Henriksen, E. A. Quintero, C. R. Harris, A. M. Archibald, A. H. Ribeiro, F. Pedregosa, and P. van Mulbregt, SciPy 1.0: Fundamental algorithms for scientific computing in Python, *Nature Methods* **17**, 261 (2020).
- [74] T. P. Peixoto, *The Netzschleuder network catalogue and repository*, Zenodo (2020).
- [75] J. Alvarez-hamelin, L. Dallasta, A. Barrat, and A. Vespignani, Large scale networks fingerprinting and visualization using the k-core decomposition, in *Advances in Neural Information Processing Systems*, Vol. 18, edited by Y. Weiss, B. Schölkopf, and J. Platt (MIT Press, 2005).
- [76] M. G. Beiró, J. I. Alvarez-Hamelin, and J. R. Busch, A low complexity visualization tool that helps to perform complex systems analysis, *New Journal of Physics* **10**, 125003 (2008).
- [77] J. I. Alvarez-Hamelin, M. G. Beiró, and J. R. Busch, Understanding Edge Connectivity in the Internet through Core Decomposition, *Internet Mathematics* **7**, 45 (2011).
- [78] E. Van Der Velden, CMasher: Scientific colormaps for making accessible, informative and 'cmashing' plots, *Journal of Open Source Software* **5**, 2004 (2020).
- [79] M. Laber, *k-Core Graph Visualization* (2025).
- [80] F. Gursoy and D. Gunnec, Influence maximization in social networks under Deterministic Linear Threshold Model, *Knowledge-Based Systems* **161**, 111 (2018).
- [81] A. K. McCallum, K. Nigam, J. Rennie, and K. Seymore,

- Automating the Construction of Internet Portals with Machine Learning, [Information Retrieval](#) **3**, 127 (2000).
- [82] M. Fire, R. Puzis, and Y. Elovici, Link Prediction in Highly Fractional Data Sets, in [Handbook of Computational Approaches to Counterterrorism](#), edited by V. Subrahmanian (Springer New York, New York, NY, 2013) pp. 283–300.
- [83] S. Kumar, F. Spezzano, V. S. Subrahmanian, and C. Faloutsos, Edge Weight Prediction in Weighted Signed Networks, in [2016 IEEE 16th International Conference on Data Mining \(ICDM\)](#) (IEEE, Barcelona, Spain, 2016) pp. 221–230.
- [84] J. Kunegis, KONECT: The Koblenz network collection, in [Proceedings of the 22nd International Conference on World Wide Web](#), WWW '13 Companion (Association for Computing Machinery, New York, NY, USA, 2013) pp. 1343–1350.
- [85] B. Karrer, M. E. J. Newman, and L. Zdeborová, Percolation on Sparse Networks, [Physical Review Letters](#) **113**, 208702 (2014).
- [86] G. Palla, I. J. Farkas, P. Pollner, I. Derényi, and T. Vicsek, Directed network modules, [New Journal of Physics](#) **9**, 186 (2007).
- [87] R. M. Ewing, P. Chu, F. Elisma, H. Li, P. Taylor, S. Climie, L. McBroom-Cerajewski, M. D. Robinson, L. O'Connor, M. Li, R. Taylor, M. Dharsee, Y. Ho, A. Heilbut, L. Moore, S. Zhang, O. Ornatsky, Y. V. Bukhman, M. Ethier, Y. Sheng, J. Vasilescu, M. Abu-Farha, J.-P. Lambert, H. S. Duewel, I. I. Stewart, B. Kuehl, K. Hogue, K. Colwill, K. Gladwish, B. Muskat, R. Kinach, S.-L. Adams, M. F. Moran, G. B. Morin, T. Topaloglou, and D. Figeys, Large-scale mapping of human protein–protein interactions by mass spectrometry, [Molecular Systems Biology](#) **3**, 89 (2007).
- [88] J. Duch and A. Arenas, Community detection in complex networks using extremal optimization, [Physical Review E](#) **72**, 027104 (2005).
- [89] J. G. White, E. Southgate, J. N. Thomson, and S. Brenner, The structure of the nervous system of the nematode *Caenorhabditis elegans*, [Philosophical Transactions of the Royal Society of London. B, Biological Sciences](#) **314**, 1 (1997).
- [90] R. Alberich, J. Miro-Julia, and F. Rossello, [Marvel Universe looks almost like a real social network](#) (2002), [arXiv:cond-mat/0202174](#).
- [91] A. Beveridge and J. Shan, Network of Thrones, [Math Horizons](#) **23**, 18 (2016).
- [92] L. Šubelj and M. Bajec, Robust network community detection using balanced propagation, [The European Physical Journal B](#) **81**, 353 (2011).
- [93] M. De Domenico, A. Solé-Ribalta, S. Gómez, and A. Arenas, Navigability of interconnected networks under random failures, [Proceedings of the National Academy of Sciences](#) **111**, 8351 (2014).